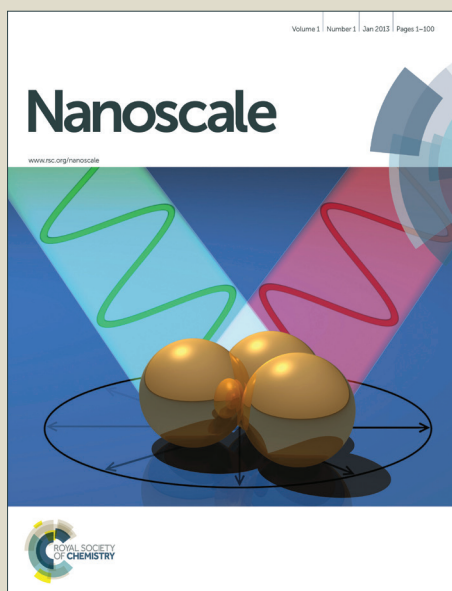


# Nanoscale

Accepted Manuscript



This is an *Accepted Manuscript*, which has been through the Royal Society of Chemistry peer review process and has been accepted for publication.

*Accepted Manuscripts* are published online shortly after acceptance, before technical editing, formatting and proof reading. Using this free service, authors can make their results available to the community, in citable form, before we publish the edited article. We will replace this *Accepted Manuscript* with the edited and formatted *Advance Article* as soon as it is available.

You can find more information about *Accepted Manuscripts* in the [Information for Authors](#).

Please note that technical editing may introduce minor changes to the text and/or graphics, which may alter content. The journal's standard [Terms & Conditions](#) and the [Ethical guidelines](#) still apply. In no event shall the Royal Society of Chemistry be held responsible for any errors or omissions in this *Accepted Manuscript* or any consequences arising from the use of any information it contains.

# Rational Design of Nanomaterials for Water Treatment

Renyuan Li, Lianbin Zhang, Peng Wang

Water Desalination and Reuse Center, Division of Biological and Environmental Science and Engineering, King Abdullah University of Science and Technology, Thuwal 23955-6900, Saudi Arabia. Corresponding email: peng.wang@kaust.edu.sa

## Abstract

The ever-increasing human demand for safe and clean water is gradually pushing conventional water treatment technologies to their limits. It is now a popular perception that the solutions to the existing and future water challenges will highly hinge upon the further development of nanomaterial sciences. The concept of rational design emphasizes 'design-for-purpose' and it necessitates a scientifically clear problem definition to initiate the nanomaterial design. The field of rational design of nanomaterials for water treatment has experienced a significant growth in the past decade and is poised to make its contribution in creating advanced next-generation water treatment technologies in the years to come. Within the water treatment context, this review offers a comprehensive and in-depth overview of the latest progress of the rational design, synthesis and applications of nanomaterials in adsorption, chemical oxidation and reduction reactions, membrane-based separation, oil-water separation, and synergistic multifunctional all-in-one nanomaterials/nanodevices. Special attention is paid on chemical concepts of the nanomaterial designs throughout the review.

## 1. Introduction

Water pollution and water scarcity are among the most severe grand challenges facing the mankind nowadays.<sup>1</sup> With rapid population growth, steadily improving life standards, fast industrialization and modernization of the developing countries, these challenges will persist, if not worsening, in the years to come.<sup>2</sup> Conventional water treatment technologies, including adsorption,<sup>3-5</sup> chemical treatment,<sup>6-9</sup> membrane based separation,<sup>10, 11</sup> biological treatment,<sup>12-14</sup> etc., are generally designed on the basis of bulk water chemistry and without any doubt, these technologies have made their critical contributions in sustaining the human society in the past century. However, the ever-increasing demand for safe and clean water is gradually pushing them to their limits.

On the other hand, ever since 1959 when the term of "nanotechnology" was first come up with by Richard Feynman in his famous lecture entitled "there's plenty of room at the bottom",<sup>15</sup> the field of nanomaterial/nanotechnology has been experiencing literally explosive growth especially in the last two decades.<sup>16-21</sup> In a traditional sense, nanomaterial has two primary advantages over conventional bulk material: (1) very small size and huge specific surface area, which are beneficial to many interface related applications;<sup>16, 22-27</sup> (2)

distinctively tunable chemical, physical, optical, electro, mechanical properties, which can be rationally adjusted by controlling its size, surface morphology, shape, crystal orientation, etc.<sup>28-34</sup> As a result, the concept of going to nanoscale has opened up many new avenues that would be otherwise impossible with the conventional bulk materials.<sup>16, 27</sup>

It is not a surprise that the nanomaterial/nanotechnology met with water treatment at one point and the application of nanomaterial to water treatment and more broadly to environmental remediation has since steadily grown into a distinct field with the expected growth rate on an exponential rise.<sup>35-45</sup> In the early stage, the concept of nanomaterial first attracted attentions from the researchers in environmental science and it was regarded having unconfirmed potentials in environmental remediation. At this stage, the major efforts have been made in directly searching for available nanomaterials developed by material scientists in a trial-and-error manner. Occasionally, material scientists also were involved in water treatment research in a bid to find some applications for their newly developed nanomaterials. Although a high level of disconnection then between the ones who synthesized the nanomaterials and the ones who tested their performances was not uncommon, these pioneering work demonstrated the great potential of nanomaterial in the water treatment field<sup>35</sup> and therefore naturally pushed it to the next stage, which can be described as rational design of nanomaterial for water treatment. In this stage, researchers realized that the chemistry and ultimate the functions of nanomaterials could be deliberately pre-designed for a desired purpose before embarking on nanomaterial synthesis. Within the scheme of rational design, less attention is paid to the inherent properties of the currently available nanomaterials and more focus is on designing and calculatedly imparting synergistic multi-functionalities to to-be-developed nanomaterials, or in some cases nanodevices, to target a clearly defined problem<sup>46-51</sup>. In this rational design stage, the nanomaterials are generally made of multi-components and the material design, synthesis and application have been seamlessly integrated within one entity to ensure the effective and iterative communication/feedback between nanomaterial design and the final performance toward well-defined purposes, which leads to high likelihood of achieving the final goals.

The focus of this review is on the rational design of nanomaterials for water treatment applications. However, the review is not intended to be exhaustive and instead it aims to give a comprehensive overview of this exciting field by using a limited number of examples. It is for this purpose that some of the topics, for examples, nano-assisted bio-remediation, nano-assisted ion-exchange, nanomaterial-based water pollutant sensors, nano-assisted microbial fuel cell, design of nanoscale zero-valent iron (NZVI) based treatment system, etc., although interesting, are not included in the review. It is worth pointing out that the review defines nanomaterials as the substances with controllable features at nanoscale, instead of on a particle size basis, which makes many materials and devices eligible for this review. The review is divided into the following sub-topics: (1) rational design of nanoporous materials and their pore structure controls, (2) rational design of nano-adsorbents by surface chemistry engineering; (3) rational design of nano-assisted oxidation and reduction processes; (4) rational design of nano-assisted membrane based separation; (5) rational design of superwetting surfaces for oil-water separation; (6) multifunctional all-in-one

nanomaterials and nanodevices for designed purposes, and (7) concluding remarks.

## 2. Rational design of nanoporous materials and their pore structure controls

As the size of a particle decreases, its specific surface area (i.e., surface area per unit mass) increases drastically (Figure 1a)<sup>52</sup> and it was the ultra-high specific surface area of nano-sized materials that first attracted attentions from the water treatment field because many water treatment processes rely on interface-related processes (e.g., adsorption, chemical reaction, catalysis),<sup>5-7, 9</sup> whose performance is positively dependent on the material surface area. Tremendous published results have demonstrated the effectiveness of the strategy of going to nano-size for enhanced performance by making smaller and smaller materials.<sup>22, 53-55</sup> As an important example, research groups all around the world demonstrated the remarkably higher degradation rate of trichloroethylene (TCE) by nanoscale zero-valent iron (NZVI) (generally with a size 10-100 nm) than by the bulk iron filings (with size > 2mm) in the conventional permeable reactive barriers (PRBs) for the same purpose.<sup>56-63</sup> The NZVI for TCE degradation heavily dominated the research of nanomaterial application to water treatment, especially groundwater treatment, in the early times.<sup>37</sup>

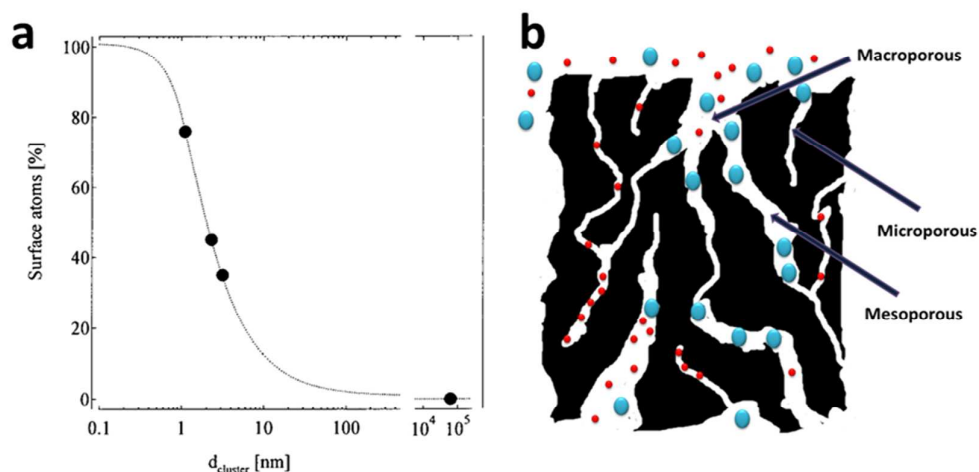


Figure 1. (a) The average percentage of surface atoms as a function of the nanoparticle diameter. Reprinted with permission from ref. 52. Copyright Springer 2000. (b) A structural scheme for a typical activated carbon, which contains highly disordered macropores (> 50nm), mesopores (2-50 nm), and micropores (< 2nm). The micropores contribute to a large part of its surface area, but are only available for the adsorption of small molecules and may be easily jammed by large molecules.

However, an inevitable downside of having nano-sized particles is the separation and recycling problems after their applications, which diverts some research attentions into making numerous nano-sized pores in big-sized materials. With a well-designed nanoporous material, the material simultaneously possesses both high surface area and reasonably large particle size, which alleviates its separation and recycling concern by a high extent. Thus, nanoporous materials have found themselves many applications in water treatment as nanoporous adsorbents,<sup>64-66</sup> nanoporous catalyst,<sup>67</sup> nanoporous hosting substrates for

nano-sized catalysts,<sup>68,69</sup> etc. Historically, activated carbon, whose surface area is generally between 500 and 1500 m<sup>2</sup>/g, is a conventional nanoporous material and has been widely utilized for water treatment in the past century.<sup>70</sup> Its ultra-high surface area along with its high stability in aqueous environment makes it an important and versatile adsorbent for a variety of water pollutants. However, the major shortcomings of the activated carbon are: (1) its pore structure is disordered and (2) the majority of its pores is within the range of micropores (pores with size  $\leq 2$  nm) (Figure 1b), which leads to its low adsorption capacity for large molecules, its sluggish mass transfer kinetics and long equilibration time. It is common that many activated carbons take days to weeks to reach their adsorption mass transfer equilibrium.<sup>70-76</sup>

Significant efforts were made in finding ordered porous silica-based nanostructures with high surface area in 1990s. In 1991, Dr. Whitesides from Harvard University highlighted the concept of self-assembly, which is the key strategy for the synthesis of various nanostructures.<sup>77</sup> In 1992, Mobil company in USA highlighted liquid-crystal template mechanism, which further facilitated the pore structure controlling and led to the creation of the well-known ordered mesoporous silica materials, MCM-41, MCM-48 and MCM-50 (commonly known as the MCM-41s), with well-ordered and uniform pore size at 2 - 8 nm.<sup>78</sup> The arising of MCM-41s demonstrates a meaningful route in preparing ordered nanoporous structures and in controlling the pore diameters by using different surfactants, adopting different hydrothermal/calcination treatment temperatures, adding micelle swelling agents, etc. Comparing with the conventional activated carbon, MCM-41s have ordered pore structure, controllable pore size, and accordant pore diameter. These advantages made the controllable nano-synthesis a very attractive method for further fabrication of new porous materials at that time. The field of pore size and pore structure control was fast moving. In 1993, the concept of cooperative self-assembly was put forward by Dr. Stucky<sup>79</sup> (Figure 2).<sup>80</sup> Five years later, a new branch of well-ordered mesoporous materials with larger pore diameter (7.5 to 32.0 nm) and thicker wall (3.1 to 6.4 nm) was fabricated in University of California, Santa Barbara (UCSB), named SBA-15, by using block-copolymer with large molecular weight as the structure directing agents.<sup>81</sup> The increase in the wall thickness increases the stability of mesoporous silica and the larger pores make feasible the adsorption of large molecules and at the same time dramatically increase the mass transfer kinetics within the pores.

In 1999, Ryoo et al. first demonstrated a fabrication of a mesoporous carbon material, CMK-1, with ordered and uniform mesoporosity by nanocasting method.<sup>82</sup> Later, a family of mesoporous carbon, named CMK-X (x= 1-9), was similarly fabricated by using different mesoporous silica as hard template and different precursor as carbon source.<sup>83</sup> The mesopores of these materials come from the removal of the silica templates and therefore correspond to the wall thickness of their mother templates, which is in the range of 1 – 4 nm.<sup>83</sup> As expected, compared with the conventional activated carbon, the mesoporous carbon showed dramatically enhanced adsorption kinetics and capacities.<sup>75</sup> In one example, ordered mesoporous carbonaceous phenol-formaldehyde resins prepared by nanocasting method exhibited adsorption capacities of 317.5 mg/g and 134.2 mg/g for fushisin and aniline respectively with adsorption equilibration time being less than 1 hour.<sup>84</sup>

However, the nanocasting synthesis of mesoporous carbon uses mesoporous silica as template, which makes it a multi-step and material-intensive procedure. In 2004, Dai et al. reported a direct synthesis of ordered mesoporous carbon by using block-copolymer as structure directing agent and resorcinol as carbon precursor via soft template method.<sup>85</sup> Soon afterwards, Zhao et al. reported an improved direct synthesis strategy of mesoporous carbon, FDU-14, FDU-15 and FDU-16, by using low molecular phenolic resin as precursor and Poloxamer type block-copolymer as structure directing agent (Figure 3a).<sup>86-88</sup> This method was then quickly extended to the synthesis of mesoporous carbon via aqueous solution, which makes it amicable for the large scale production.<sup>89</sup> Up to now, the pore size of the FDU family of mesoporous carbon can be readily tuned from 12 to 37 nm, which opens up a lot of applications for them.<sup>90-93</sup>

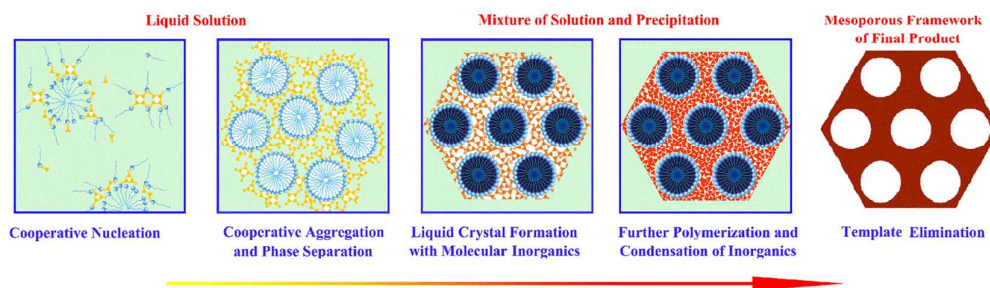


Figure 2 The formation of mesoporous material via cooperative self-assembly strategy. In the first step, surfactants and inorganic species are attracted together due to the interaction coming from hydrogen bond or electrostatic attraction; in the second step, the continuous hydrolysis and crosslinking of the inorganic species cause further cooperative aggregation and eventually lead to phase separation from the solution; in the third step, the surfactant-inorganic species form ordered mesostructure to decrease the total interfacial energy; the fourth step involves further polymerization and condensation of inorganic species. Upon the surfactant removal, the final mesoporous product is obtained. Reprinted with permission from ref. 80. Copyright American Chemical Society 2007.

The great progress on the synthesis of mesoporous silica and carbon with controllable, uniform and large pore size (Figure 3b) provides these materials plenty of opportunities in water treatment. The removal of microcystins from water by adsorption is an insightful example. It is well known that microcystins are extremely toxic with a large molecular weight of about 1000 Da and large size of 1-2 nm, and they are usually produced in cyanobacterial blooms occurring in many eutrophic waters.<sup>94</sup> Activated carbon has been adopted for the adsorption of microcystins and it is found that the small micropores of the activated carbon do not contribute to the adsorption due to the molecular sieve effect.<sup>95</sup> In 2007, Zhao et al. employed a mesoporous silica with a pore size of 2.3 nm to adsorb microcystins and found that over 95.4% of the microcystins was removed and adsorbed onto the silica within 60 seconds, which stood in a drastic contrast against very slow adsorption of microcystins on the activated carbon.<sup>96</sup> In 2013, the same group compared the microcystins adsorption on a series of mesoporous silica with different pore size and pore structure, and found that the

mesoporous silica with larger mesopores ( $> 6$  nm) had a much higher adsorption capacity than those with small mesopores (2-3 nm). In one case, SBA-15 with a pore size of 8.7 nm, despite its smaller specific surface area ( $800 \text{ m}^2/\text{g}$ ), exhibited a microcystins adsorption capacity six times that of MCM-41 with a pore size 2.8 nm and surface area  $1180 \text{ m}^2/\text{g}$ .<sup>97</sup> This result convincingly demonstrates the necessity and effectiveness of pore size engineering. However, due to the weak surface interaction between microcystins and silica, the microcystins adsorption capacity on mesoporous silica is far from being satisfying. Recently, ordered mesoporous carbon was utilized and showed improved performance for microcystins adsorption. An ordered mesoporous carbon with bimodal mesopores (2.8 and 5.8 nm), a surface area of  $1680 \text{ m}^2/\text{g}$  and pore volume of  $1.67 \text{ cm}^3/\text{g}$ , exhibited an unprecedented microcystins adsorption capacity of  $526 \text{ mg/g}$ , which was 30 times that of the powder activated carbon tested under the otherwise same conditions.<sup>75</sup>

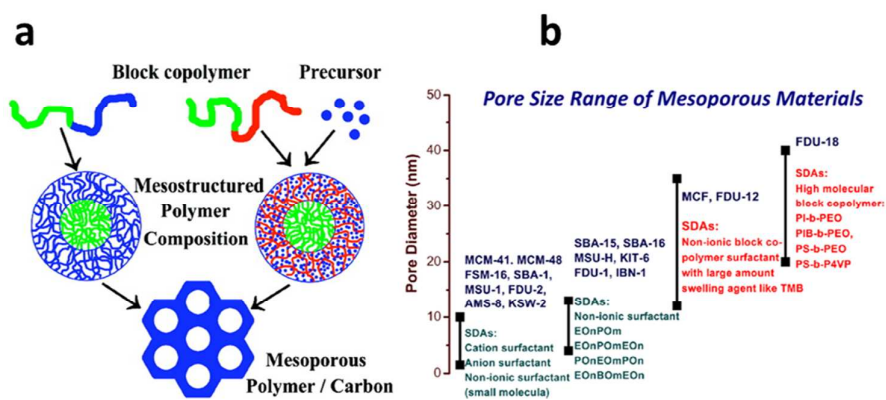


Figure 3 (a) Two strategies for the direct synthesis of mesoporous carbon by using block copolymer as structure directing agent. In the first strategy (left), one block of the block copolymer is used as the carbon source and the other block is selectively removed to form uniform mesopores. In the second strategy (right), the carbon precursor is separately added and the entire block copolymer is removed after the carbonization process. Reprinted with permission from ref. 88. Copyright American Chemical Society 2008. (b) Classification of Mesoporous materials according to their pore size distribution and the surfactant used in their synthesis.

In the past decade, ultra-thin two dimensional (2D) solids, defined as crystals with very high aspect ratios and thicknesses corresponding to a single or few atomic layers, have attracted tremendous research attentions<sup>98</sup> due to their extremely high surface atom ratio along with other attractive features. In water treatment, the 2D materials are particularly appealing majorly for the following reasons: (1) the ultra-thin layer structure of the 2D materials endows them with a high specific surface area and stable structures. For example, the surface area of monolayer graphene is around  $2630 \text{ m}^2/\text{g}$ ;<sup>99</sup> (2) the edges and defects sites on the layers of the 2D materials can be conveniently functionalized; (3) when stacked together, they form a tight structure but with a controllable interlayer space, which is desirable for many design purposes;<sup>100, 101</sup> (4) in practice, few-layer-stacked 2D structures-based materials can be facily synthesized, from which various types of bulk materials can be made, such as membrane, powder, fiber, etc.<sup>100, 101, 102</sup> Among them,

graphene, an atomic monolayer consisting of densely packed carbon atoms, along with its derivatives (especially graphene oxide (GO) and reduced graphene oxide (rGO)), are by far the most studied 2D materials.<sup>98</sup> Due to its ultra-thin wall thickness, graphene-based ultra-porosity sponge with extremely high pore volume has been showed very effective as oil sorbents, removing as many as 69 times oil that of its own weight.<sup>102,103,104</sup>

In 2011, a new and exciting group of 2D materials composed of early transition metal carbides and/or carbonitrides now known as MXenes, was introduced by Gogotsi's group<sup>105</sup> and its family has been growing henceforth, along with its application prospective.<sup>98</sup> MXenes are produced by etching out of the A layers from MAX phases, where M is an early transition metal, A is mainly a group IIIA or IVA (i.e., groups 13 or 14) element, X is C and/or N, and  $n = 1, 2, \text{ or } 3$ .<sup>98,106</sup> The natural tendency of adsorbing cationic ions onto their surfaces and the high surface area endow MXenes highly desired properties in energy storage and water treatment areas.

### 3. Rational design of nano-adsorbents by surface chemistry engineering

Nanoporous, especially well-ordered mesoporous materials, are cut out for excellent adsorbents, given their high surface areas, large and regularly ordered mesoscale channels, and thus fast mass transfer kinetics.<sup>75,96,97,107</sup> However, a high and fast adsorption relies not only on a high surface area to provide active adsorption sites and unobstructed pathways for the adsorbates to quickly reach their adsorption sites, but also on the interaction between the active sites and the targeted adsorbates, which controls the strength and the selectivity of the adsorption.<sup>108,109</sup> While the surfaces of carbon based nanoporous materials are largely chemically inert and thus difficult to functionalize, the surfaces of silica materials are covered by silanol groups, which only provide weak interactions with polar adsorbates, leading to quite limited adsorption capacity and unsatisfactory selectivity. However, given their well-known rich chemistry, silica surface and silanol groups are amicable to a variety of chemical modifications also due to the wide availability of various organosilane coupling reagents.<sup>108-110</sup> Therefore, in parallel with pore size and pore structure engineering, the surface chemical functionalization, especially of nanoporous silica based materials, is also a basis of many rational designs of nano-adsorbents for water pollutant removal.

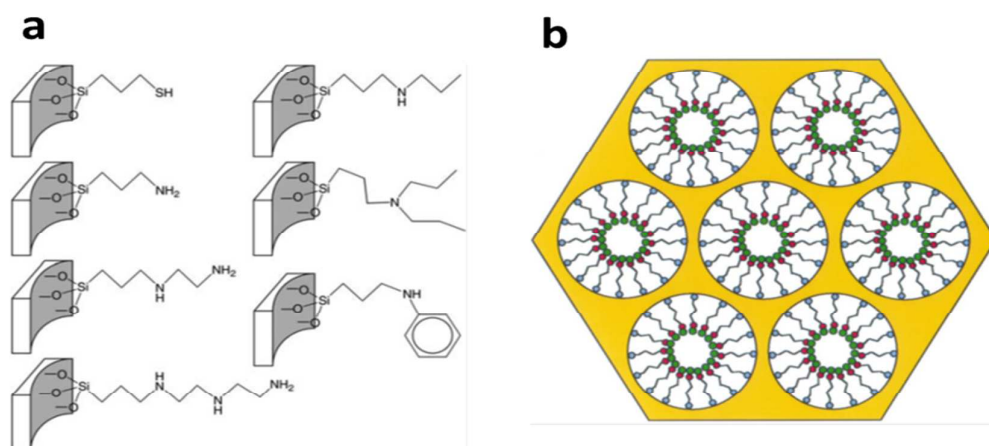


Figure 4. (a) Several commonly used organo-functional groups grafted on the pore surface via Si-O-Si covalent bonds for the preparation of mesoporous silica-based adsorbents. Reprinted with permission from ref. 108. Copyright Royal Society of Chemistry 2010. (b) The scheme illustrates the structure model of self-assembled monolayers on mesoporous supports (SAMMS) adsorbent with a monolayer functional group (red dots) on its mesopore surface, which shows efficient adsorption of the aimed metal ion pollutants (green dots). Reprinted with permission from ref. 117. Copyright American Association for the Advancement of Science 1997.

### 3.1 Charged species removal

**Cationic heavy metal removal.** Typically, for cationic pollutants, especially cationic heavy metals, such as copper ( $\text{Cu}^{2+}$ ), zinc ( $\text{Zn}^{2+}$ ), mercury ( $\text{Hg}^+$ ), lead ( $\text{Pb}^{2+}$ ), cadmium ( $\text{Cd}^{2+}$ ), they can serve as central cations in a complex with various ligands (e.g.,  $-\text{NH}_2$ ,  $-\text{SH}$ ), which provides a very strong interaction between the central cations and the ligands.<sup>111</sup> Generally, a soft ion, such as  $\text{Hg}^{2+}$ , is more likely to form a more stable complex with a ligand that contains a soft electron donor atom, such as thiol, and vice versa.<sup>109, 112</sup> This principle helps design the adsorbents with judiciously chosen ligand groups to selectively target cationic metal pollutants from a complex matrix.

Most of the functional ligand groups can be easily linked to the surface of mesoporous silica by grafting the organosilanes with corresponding terminal groups via  $-\text{Si-O-Si}-$  covalent bond (Figure 4a).<sup>108, 113</sup> The surface grafting can be achieved either by post-grafting strategy or by one-pot co-condensation strategy, and both of them have been well developed in the last decades.<sup>114-116</sup> One successful example is the mesoporous silica materials functionalized with thiol-based ligand groups (thiol, thiourea, thioether, etc.) on their pore surfaces for the removal of  $\text{Hg}^{2+}$  by adsorption.<sup>109, 112, 117</sup> These rationally designed adsorbents show extremely high capacity, fast kinetics, and high selectivity over common competing metal cations due to the specific complex chemistry between  $\text{Hg}^{2+}$  and thiol-based groups, in which the Hg to  $-\text{SH}$  molar ratio can be as high as 1.0. In 1997, Liu et al. synthesized a mesoporous silica material and grafted its pore surface with (methoxy)mercaptopropylsilane to achieve 76% coverage of the pore surface with  $-\text{SH}$  groups (Figure 4b), and the synthesized material exhibited a high  $\text{Hg}^{2+}$  adsorption capacity of 505 mg/g.<sup>117</sup> In addition to the post grafting method, also feasible is  $-\text{SH}$  group introduction onto the pore surface of mesoporous silica by one-pot co-condensation strategy with even higher  $-\text{SH}$  group loading (4.1 mmol/g), which led to an adsorption capacity of  $\text{Hg}^{2+}$  to more than 800 mg/g in one case.<sup>118</sup>

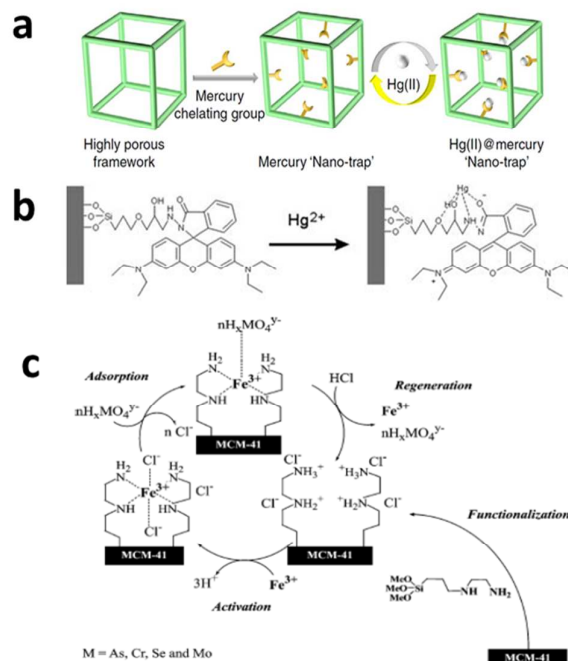


Figure 5 (a) A highly efficient adsorbent with mercury nano trap is fabricated by linking the mercury chelating group  $-SH$  to a highly porous aromatic framework PAF-1, which has a Langmuir surface area of  $7100 \text{ m}^2/\text{g}$ . The product shows high adsorption capacity and can be easily regenerated for reuse. Reprinted with permission from ref. 123. Copyright Nature Publishing Group 2014. (b) A proposed model for the selective binding of  $\text{Hg}^{2+}$  with a specially designed ligand with fluorescence group, which makes it a  $\text{Hg}^{2+}$  sensor as well as a selective adsorbent. Reprinted with permission from ref. 122. Copyright Royal Society of Chemistry 2010. (c) A mesoporous silica-based adsorbent with amino groups on its pore surface. After it chelates with  $\text{Fe}^{3+}$ , the adsorbent shows high affinity with oxyanionic heavy metal pollutants and can be regenerated by HCl washing. Reprinted with permission from ref. 142. Copyright Elsevier Inc. 2004.

In 2000, Kawi et al. compared thiol- and amino-functionalized SBA-15 silica for the adsorption of heavy metal ions and found that the thiol-functionalized SBA-15 showed high removal efficiency for  $\text{Hg}^{2+}$ , but were much less successful for  $\text{Cu}^{2+}$ ,  $\text{Zn}^{2+}$ ,  $\text{Cr}^{3+}$  and  $\text{Ni}^{2+}$  due to the mismatch of coordination chemistry.<sup>119</sup> On the other hand, the amino-functionalized SBA-15 showed good removal efficiency for all ions but  $\text{Hg}^{2+}$ . However, because the binding strength between amino-groups and these metal cations ( $\text{Cu}^{2+}$ ,  $\text{Zn}^{2+}$ ,  $\text{Cr}^{3+}$ ,  $\text{Ni}^{2+}$ ,  $\text{Hg}^{2+}$ ) are much weaker than that between thiol-group and  $\text{Hg}^{2+}$ , amino-functionalized adsorbents only lead to a low capacity and poor selectivity in comparison to thiol-functionalized ones for  $\text{Hg}^{2+}$  removal. For example, the maximum adsorption capacities of  $\text{Ni}(\text{II})$ ,  $\text{Cd}(\text{II})$  and  $\text{Pb}(\text{II})$  ions with a  $-\text{NH}_2$  group functionalized mesoporous silica MCM-41 were only 12.4, 18.3 and 57.7 mg/g, respectively.<sup>120</sup> In an attempt to further increase the binding strength between amino group and the metal ions, melamine-based dendrimer amines were utilized as the functional groups to modify SBA-15 and the functionalized SBA-15 exhibited adsorption capacities of

130, 126 and 98 mg/g for Pb(II), Cu(II) and Cd(II), respectively.<sup>121</sup>

In 2010, Tao et al. functionalized the surface of a mesoporous silica with a complex amino group (-CH<sub>2</sub>-CH<sub>2</sub>-O-CH<sub>2</sub>-CH(OH)-CH<sub>2</sub>-NH<sub>2</sub>), which was further reacted with Rhodamine B to form a complicated ligand as shown in Figure 5b.<sup>122</sup> Interestingly, unlike the general amino-functionalized mesoporous silica, this material exhibited a high selectivity for Hg<sup>2+</sup> from an aqueous matrix containing Na<sup>+</sup>, Mg<sup>2+</sup>, Mn<sup>2+</sup>, Co<sup>2+</sup>, Ni<sup>2+</sup>, Zn<sup>2+</sup>, Cd<sup>2+</sup>, Ag<sup>+</sup>, Pb<sup>2+</sup>, and Cu<sup>2+</sup>. Although the mechanism behind the high selectivity in this case is not fully understood, the results of this work hint that, beyond the simple groups as discussed above, the design of more complicated ligands may provide some unprecedented opportunity to achieve exclusive binding to target heavy metal cations of interest with high selectivity.

One shortcoming of the silica-based materials is the poor stability of -Si-O-Si- bond in base condition, which may cause the leaching of the surface-grafted functional groups.<sup>123</sup> Very recently, Li et al. reported a thiol functionalized porous organic polymer based nano-trap for selective Hg<sup>2+</sup> removal and the material achieved an Hg<sup>2+</sup> adsorption capacity over 1000 mg.g<sup>-1</sup> along with a high selectivity and a fast adsorption kinetics (Figure 5a).<sup>123</sup> More importantly, this material showed high stability in water under a wide pH range attributed to its stable C-C bond and it remained stable at high temperature up to 270 °C. Other abundant and inexpensive polymers, such as polystyrene, polysaccharide, have also been tested in adsorption applications and showed good performances in the removal of heavy metals, organic dyes, organic compounds, etc.<sup>124, 125</sup>

Metal oxides besides SiO<sub>2</sub> were also examined for their potentials in cationic pollutant adsorption. For example, Dubey et al. reported manganese oxide nanoparticles as good adsorbent for Hg<sup>2+</sup>.<sup>126</sup> Afkhami et al. reported 2,4-dinitrophenylhydrazine modified aluminum oxide nanoparticles which showed the adsorption capacity of Pb(II) at 100 mg/g, Cd(II) at 83 mg/g, and Co(II) at 41 mg/g.<sup>127</sup> Their adsorption ability can be ascribed to electrostatic attraction between these metal oxide adsorbents and cationic heavy metal ions.<sup>128</sup>

Recently, the 2D materials have been employed in adsorption. For example, Xie et al. reported a graphene oxide aerogel with a Cu<sup>2+</sup> adsorption capacity of 19 mg/g.<sup>129</sup> Sampeth et al. investigated the dye adsorption and found that cationic dye had higher adsorption onto exfoliated graphene oxide while rGO favored anionic dye.<sup>130</sup> In 2014, Zhang et al. developed a large scale preparation method of MXenes and the produced MXenes were able to selectively reduce the aqueous Pb<sup>2+</sup> concentration lower than 2 ug/L. In this study, the strong selectivity was attributed to strong metal-ligand interaction between [Ti-O]<sup>-</sup>H<sup>+</sup> groups and Pb(II), large surface area of the MXenes led by HF exfoliation, and the lower hydration energy of Pb(II) comparing with other cations such as Ca(II) and Mg(II), which leads to Pb(II) more easier adsorb onto OH-rich surface.<sup>131</sup> While the exact adsorption mechanism remains to be further explored and confirmed, MXenes have shown good adsorption performances for Cr and dyes.<sup>132, 133</sup>

**Oxyanion removal.** Another group of heavy metals, such as arsenic and chromium, tend to form various negative charged oxyanions in aqueous environment as a function of their valence state and the environmental conditions (e.g. pH). For example, depending on

aqueous pH, common species of arsenic ion in water include such oxyanions as  $\text{AsO}_4^{3-}$ ,  $\text{H}_2\text{AsO}_4^-$ ,  $\text{HAsO}_4^{2-}$  for As(V) and  $\text{As}(\text{OH})_3$ ,  $\text{As}(\text{OH})_4^-$ ,  $\text{AsO}_2\text{OH}^{2-}$  and  $\text{AsO}_3^{3-}$  for As(III)<sup>134</sup>. In the structures of these oxyanions, the metal cations are surrounded by oxygen and their orbitals are generally fully occupied.<sup>111</sup> As a result, achieving specific binding of these oxyanion species on adsorbents is theoretically challenging. So far, the basic strategy to remove these overall negatively charged groups is utilizing electrostatic attraction by positively charged surfaces.<sup>134-137</sup> Given their positive charges under acidic condition, amino-based groups are the most popular choice for the surface modification. As expected, the effectiveness of this strategy is highly dependent on environmental conditions (e.g., pH, ionic strength, presence of competing species) and it has a poor selectivity due to the nature of weak electrostatic interaction.<sup>138</sup>

In 1992, Ramana et al. found that the copper-chelated pyridyl and tertiary ammonium polymers exhibited a high affinity toward arsenate ( $\text{AsO}_3^{3-}$ ) due to the ultralow solubility of cupric arsenate.<sup>139</sup> In 1999, Liu et al. designed a strategy for the adsorption of arsenate and chromate ( $\text{CrO}_4^{2-}$ ) by using similar metal-chelated ligands as active sites,<sup>140</sup> in which ethylenediamine group was firstly grafted onto the surface of mesoporous silica and then chelated with  $\text{Cu}^{2+}$ . This metalized adsorbent exhibited a high adsorption capacity of 142 mg/g for arsenate and 132 mg/g for chromate. It was proposed that in the course of adsorption, the aimed oxyanions, arsenate or chromate, would directly bind to the  $\text{Cu}^{2+}$  ions by releasing one of three ethylenediamine ligands that previously chelated with the  $\text{Cu}^{2+}$  and the oxyanions would thus be locked in the complex trap formed by the  $\text{Cu}^{2+}$  and ethylenediamine ligands.

In 2003, Tatsumi's group investigated this kind of metalized adsorbents in more details by using three different amino groups as the ligands, namely,  $-\text{NH}_2$  (1N),  $-\text{NH}-\text{CH}_2-\text{CH}_2-\text{NH}_2$  (2N) and  $-\text{NH}-\text{CH}_2-\text{CH}_2-\text{NH}-\text{CH}_2-\text{CH}_2-\text{NH}_2$  (3N), and  $\text{Fe}^{3+}$ ,  $\text{Co}^{2+}$ ,  $\text{Ni}^{2+}$ , and  $\text{Cu}^{2+}$  as the metal additives.<sup>141</sup> It was found that  $\text{Fe}^{3+}$  exhibited the best performance due to the strong interaction between iron and arsenic (Figure 5c). In case of MCM-48 as the matrix, 2N group as the ligand and  $\text{Fe}^{3+}$  as the metal additive, one  $\text{Fe}^{3+}$  bound to about 2.7 arsenate anions and the final arsenic adsorption capacity was as high as 353 mg/g. In 2004, the same group further demonstrated the high adsorption capacities of the same materials for chromate (115 mg/g), selenate (116 mg/g) and molybdate (206 mg/g).<sup>142</sup>

As mentioned above, iron ions form very strong binding interaction with arsenate and chromate, and therefore all kinds of iron-containing materials, such as zero-valent iron, iron oxides, iron oxyhydroxides, iron hydroxides, have been utilized for the removal of arsenic and chromium in the last two decades<sup>134</sup> and they are regarded as promising adsorbents due to their natural abundance, low cost and non-toxicity. In 2000, Lackovic et al. demonstrated that both As(III) and As(V) could be effectively removed from aqueous solution by zero-valent iron due to the surface precipitation or complexation of arsenic with iron.<sup>143</sup> By making smaller and smaller iron-containing nanoparticles, the adsorption capacity of arsenic has been greatly improved. In 2006, Yavuz et al. synthesized monodispersed  $\text{Fe}_3\text{O}_4$  nanoparticles with diameters of 12 nm, which exhibited a high arsenic adsorption capacity of 200 mg/g.<sup>22</sup> Such a high capacity is mainly attributed to the high fraction of exposed iron on the surface of these ultra-small particles. However, the ultra-small particles have strong

tendency to agglomerate, which reduces their specific surface area and thus adsorption capacity.<sup>144</sup> Several strategies have recently been developed to overcome this challenge. In 2009, Lo and Wang synthesized a mesoporous  $\gamma$ -Fe<sub>2</sub>O<sub>3</sub> with self-supported porous framework, with a particle size larger than 200 nm and the pore wall thickness smaller than 10 nm, which obtained a chromate adsorption capacity of 15.6 mg/g.<sup>145</sup> In 2014, a mesoporous cerium iron mixed oxide material was similarly synthesized and exhibited adsorption capacities of ~106.2 and ~75.4 mg/g for arsenate and chromate, respectively.<sup>146</sup> In addition to making self-supported mesoporous framework, recently explored was an alternative strategy of loading ultra-small iron nanoparticle into a high surface nanoporous substrate to avoid particle aggregation. Zhao et al. loaded Fe<sub>2</sub>O<sub>3</sub> nanoparticle with size less than 10 nm in a mesoporous carbon matrix with high loading amount of 52 wt%, and the arsenic adsorption capacity of this composite material was 29.4 mg/g.<sup>147</sup> Yu et al. designed a structure in which ultra-small  $\gamma$ -Fe<sub>2</sub>O<sub>3</sub> nanoparticles (6 nm) were well dispersed within mesoporous silica foam with a pore size of around 100 nm and pore volume of 1.6 cm<sup>3</sup>/g.<sup>148</sup> The non-agglomeration of  $\gamma$ -Fe<sub>2</sub>O<sub>3</sub> in the structure maintained a high level of active adsorption sites, leading to high adsorption capacities of As (III) at 320 mg/g and As (V) at 248 mg/g. In addition, the large particle size and large pore size of the hosting silica foams ensured fast adsorption kinetics and made possible of a direct packing of the materials into a filter cartridge for household drinking water treatment at ambient pressure.<sup>148</sup>

Beside the strong interaction between Fe species with As and Cr oxyanions, some other strong interactions between metal oxide and anionic ions were also discovered and utilized.<sup>128</sup> For example, it is known now that iron oxide, magnesium oxide, zirconium oxide, and alumina, all possess strong interactions with fluoride and the nanostructures of these metal oxides have been utilized for fluoride adsorption.<sup>128</sup> Ahn et al. compared mesoporous alumina and activated alumina and concluded that the large surface area and mesopore size of the mesoporous alumina were desirable for high fluoride adsorption capacity and fast adsorption kinetics.<sup>149</sup> Chen et al. employed zirconium oxide nanoparticles for fluoride removal and achieved a capacity of 78 mg/g.<sup>150</sup> It has also been reported that zirconium phosphate (ZrP) can effectively remove trace fluoride from contaminated water.<sup>150</sup> Zhang et al. designed porous polystyrene encapsulated zirconium phosphate nanocomposite and the material showed high selectivity towards fluoride in a matrix with high concentrations of SO<sub>4</sub><sup>2-</sup>, NO<sub>3</sub><sup>-</sup>, and Cl<sup>-</sup>.<sup>151</sup>

### 3.2 Charge-neutral species removal

Hydrophobic organic compounds (HOCs), including polychlorinated biphenyls (PCBs), polycyclic aromatic hydrocarbons (PAHs) and hydrophobic pesticides, are one important category of water pollutants.<sup>152-154</sup> Their primary removal strategy is based on the principle of like dissolves like by extraction with hydrophobic medium. Activated carbons are the most widely applied adsorbents for HOC removal, but it suffers from its large fraction of micropores. Surfactant micelles have a capability of extracting HOCs from contaminated water by solubilizing HOCs within their very hydrophobic cores, but they cannot be directly separated from water.<sup>155-157</sup>

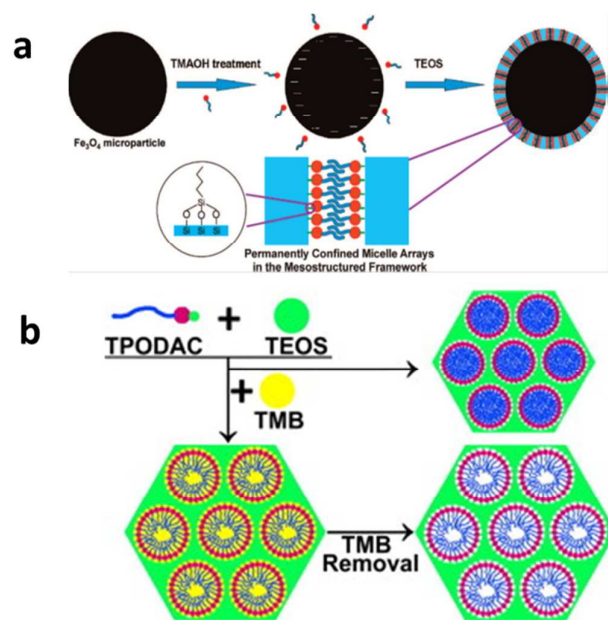


Figure 6 (a) The synthesis procedure for the Mag-PCMA, which is designed for the removal of HOCs. The mesostructured hybrid shell layer is constructed by mesoporous silica framework with the micelle arrays formed by a special surfactants with active  $-\text{Si}(\text{OCH}_3)_3$  end group inside the mesopores. In this material, the surfactant micelles are permanently anchored in the silica framework via Si-O-Si bond, which solves the surfactant leaching problem. Reprinted with permission from ref. 160. Copyright American Chemical Society 2008. (b) By using the micelle swelling agent trimethylbenzene (TMB) in the synthesis of PCMA and removing the TMB after the synthesis, additional cavities can be created inside the confined micelle arrays and thus significantly increase the HOC removal efficiency. Reprinted with permission from ref. 161. Copyright Elsevier Inc. 2012.

In 1992, mesoporous silica was first synthesized via cooperative self-assembly between surfactants and silica<sup>79</sup> and the as-made materials before calcination can be regarded as unconfined micelle arrays that are solidified by silica matrix via weak electrostatic interaction. In the late 1990s, Denoyel et al. demonstrated that these hybrid materials gave a high efficiency in removing various chlorophenols from aqueous solution.<sup>158, 159</sup> However, the problem of surfactant leaching out of these hybrid materials during the adsorption and regeneration process inhibited their practical applications. In 2008, one work from UCSB rationally designed a magnetic permanently confined micelle arrays (Mag-PCMA) to overcome the surfactant leaching problem (Figure 6 a).<sup>160</sup> In their design, a special surfactant, 3-(trimethoxysily) propyl-octadecyldimethylammonium chloride (TPODAC), which is able to form covalent bonds with silica framework, was utilized in the cooperative self-assembly and therefore the micelle arrays, once formed, were permanently solidified within the silica frameworks by covalent bonds. Due to the permanent confinement of the micelles, Mag-PCMA can be easily regenerated by simple solvent washing without losing their HOC adsorption capacity and due to the magnetic core of this core-shell structured nanomaterial,

Mag-PCMA works well in *ex situ* soil washing as well. Some co-workers later applied micelle-swelling strategy during the material synthesis (Figure 6b) and created extra space inside the permanently confined micelles, which led to an increase in the HOC adsorption capacity by as much as 3.5 times.<sup>161</sup> Cai et al. synthesized a similar core-shell magnetic mesoporous silica adsorbent by a two-step method and the final product exhibited good performance for PAHs removals.<sup>162</sup>

Comparing with many good material designs for HOCs removal, the adsorption of charge-neutral hydrophilic pollutants with environmental significance, such as pharmaceuticals and personal care products (PPCP) and dissolved natural organic matter (NOM), is always challenging and problematic. A few attempts were made by using carbon-based materials, such as activated carbon, ordered mesoporous carbon, and some of these materials showed good performance towards PPCPs adsorption.<sup>163-165</sup> However, these carbon materials are nonselective and versatile adsorbents and thus their application to this end is not within the rational design domain. The sluggish progress in the hydrophilic water pollutant adsorption is not due to lack of the efforts, but the intrinsic hydrophilicity of these compounds that makes them reluctant to leave water. Based on the principle of like dissolves like, good adsorbents toward the charge-neutral hydrophilic pollutants can be these materials whose hydrophilicity is so that it maximizes its differences with water but at the same time minimizes its difference with the pollutants of interest, which, however, hasn't been proved by any work. Molecular recognition based adsorption has shown some promise for the removal of this group of water pollutants, but it is still too early to draw any definite conclusions.

### 3.3 Molecular recognition based adsorption

Adsorption based on molecular recognition has gained some attentions in the past decade, with aptamer and molecular imprinting approaches being two good examples.<sup>166-168</sup> The commonality of all molecular recognition approaches lies in the use of the target pollutant species as a template to select or create the adsorbent that has capability of precisely recognize and more importantly select the target from a wide range of species even with similar structures.

Aptamer is a type of recently developed new ligand that can exhibit highly specific and strong affinity to the target molecule with multiple interaction points from three-dimensional directions.<sup>169, 170</sup> For a specific target molecule, a special aptamer can be screened exclusively for the target from a huge library of DNA molecules containing randomly created sequences via the systematic evolution of ligands by exponential enrichment (SELEX), also known as *in vitro* selection.<sup>171, 172</sup> This strategy has been adopted in various research areas such as nanomaterial synthesis, sensor development and has recently been utilized in water treatment. In 2009, Kim et al. selected eight aptamers from a random DNA library for arsenic (As(V) and As(III)) binding via SELEX<sup>171, 172</sup> and the selected aptamers showed extremely high affinity to both As(V) and As(III) with nanomolar scale dissociation constant ( $K_d$ ) at 4.95 and 7.05 nM, respectively.<sup>173</sup> When immobilized on streptavidin agarose resin, the aptamers removed almost all arsenic from the contaminated natural water from Vietnam with an excellent selectivity to arsenic. In 2011, Zhou et al. utilized the same strategy for the removal of trace (ng/L) pharmaceuticals of cocaine and diclofenac from

drinking water and obtained a removal efficiency as high as 88-95% (Figure 7a).<sup>174</sup>

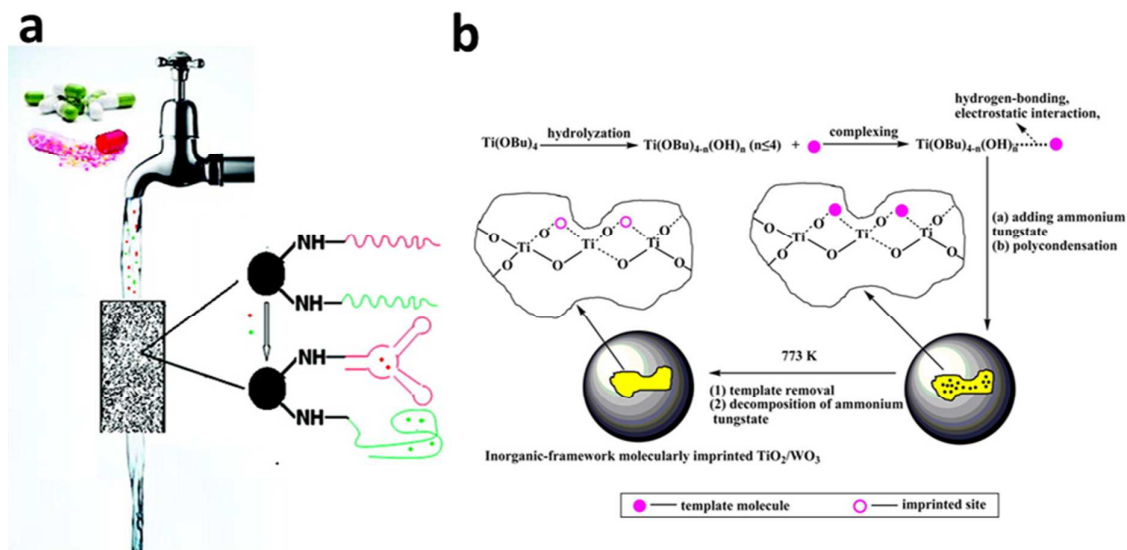


Figure 7 (a) A column packed with the adsorbents functionalized with selected aptamer, showed the ability to removal trace amount (ng/L) pharmaceuticals (e.g., cocaine and diclofenac) in drinking water with 88–95% removal efficiency. Reprinted with permission from ref. 174. Copyright American Chemical Society 2011. (b) The synthesis procedure of an inorganic-framework molecularly imprinted  $TiO_2/WO_3$  nanocomposites. The synthesized product showed selective and high photo-degradation rate for 2-nitrophenol (2NP) or 4-nitrophenol (4NP), depending on the molecular template used in the synthesis process. Reprinted with permission from ref. 110. Copyright American Chemical Society 2013.

Based on the lock-and-key mechanism used by enzyme for substrate recognition, molecular imprinting concerns with employing a target molecule as template to create template-shaped cavities in matrix, generally polymeric and in some cases inorganic, with memory of the template molecule.<sup>166-168</sup> Like aptamer-based one, the molecular imprinting strategy has high selectivity and affinity towards the template molecule even in the presence of interfering substances that may be thousands to millions of times more abundant than the target.<sup>166, 168</sup> One significant effort in molecular imprinting for water treatment concerns the development of the core-shell structured nanocomposites, consisting of magnetic-nanoparticle core and molecular-imprinted-polymer shell, for selective adsorption of water pollutants. Li et al. reported a synthesis of a core-shell magnetic molecularly imprinted polymer by the surface RAFT polymerization for fast and selective detection and removal of endocrine disrupting chemicals, such as Bisphenol A, from aqueous solutions.<sup>175, 176</sup> Other nanocomposites with similar magnetic core-shell structure were developed for the selective removal of herbicides from water,<sup>177</sup> creatinine, albumin, and lysozyme from urine,<sup>178</sup> 4-chlorophenol from water,<sup>179</sup> methyl parathion from soil solution,<sup>180</sup> and so on.

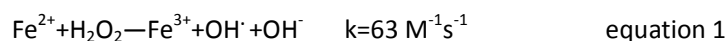
Recently, the concept of molecular imprinting has been extended to the field of photocatalysis to overcome the general non-selectivity issue especially in  $TiO_2$  based

photocatalysis. In 2007, Tang and Zhu coated a molecular imprinted polymer on the surface of TiO<sub>2</sub>-type photocatalyst P25 and identified the selective decomposition of the target pollutants in the presence of high-level interfering substances.<sup>181</sup> For example, in case of 4-chlorophenol (4CP) was used as the template, the molecular-imprinted-polymer-coated-TiO<sub>2</sub> showed a much faster reaction in decomposing 4CP than phenol ( $k_{4CP}/k_{phenol} = 20.6$ ), while for the original P25, the  $k_{4CP}/k_{phenol}$  was only 8.68. The same group also extended this method to 2-nitrophenol, 4-nitrophenol and salicylic acid, and achieved high activity and selectivity toward the photo-degradation of the targets.<sup>182, 183</sup> The effectiveness of this strategy has also been proven by other groups on the selective decomposition of 2-nitrophenol and 4-nitrophenol using inorganic-framework molecularly imprinted TiO<sub>2</sub>/WO<sub>3</sub> nanocomposites as photocatalyst (Figure 7b).<sup>110</sup>

#### 4. Rational design of nano-assisted oxidation and reduction processes

##### 4.1 Nano-assisted advanced oxidation processes

Chemical processes account for a significant fraction in conventional water treatment technologies, among which advanced oxidation processes (AOP) have been playing an important role in wastewater treatment especially in developed countries particularly for organic pollutant decomposition since its inception in late 19<sup>th</sup> century.<sup>6-9, 184, 185</sup> In a Fenton reaction, a typical AOP, peroxides (usually H<sub>2</sub>O<sub>2</sub>) react with iron ions to form highly reactive hydroxyl radicals (OH<sup>·</sup>) as described in Equations 1 and 2.<sup>186</sup> The OH<sup>·</sup> is one of the most powerful oxidants known to us whose oxidation potential ( $E = 2.80$  V) is even higher than atomic oxygen (2.42 V) and ozone (2.07 V)<sup>187</sup> and thus is capable of oxidizing most organic pollutants present in wastewater.<sup>184</sup>



A conventional Fenton reaction is carried out in a homogeneous catalysis system whose advantages include the readily available iron ions, negligible mass transfer limitations, and thus high reaction efficiency.<sup>186, 188-190</sup> However, the conventional homogeneous Fenton reaction has to take place in an acidic aqueous solution with pH generally lower than 3 to optimize the performance and to avoid losing iron ions by precipitation<sup>186</sup> (Figure 8a and 8b). The acidification of the entire bulk water before the reaction and adjusting it back to neutral pH after the reaction adds to the operation cost of the conventional Fenton system.

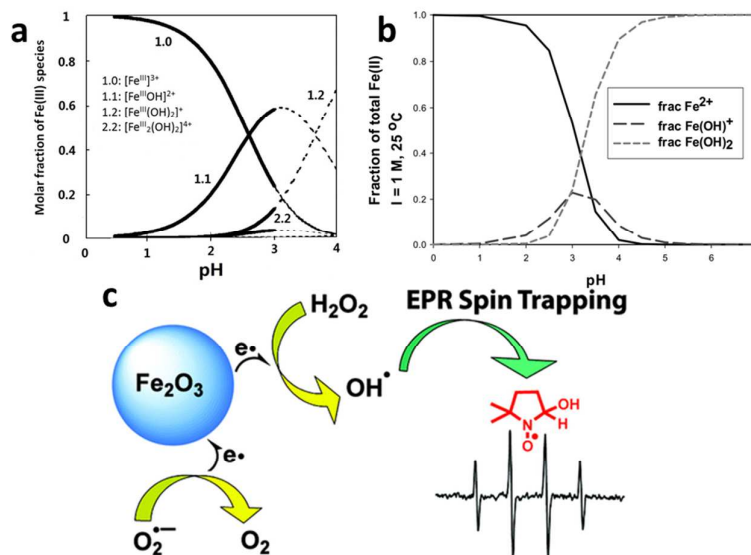


Figure 8 (a<sup>191</sup>, b<sup>192</sup>) The speciation of different  $\text{Fe}^{3+}$  and  $\text{Fe}^{2+}$  species in acidic aqueous solution at different pHs, showing that precipitation forms as the pH is higher than 4. Reprinted with permission from ref. 1191, Copyright Elsevier Inc. 1999, and reprinted with permission from ref. 192, Copyright Royal Society of Chemistry 1968, respectively. (c) A newly proposed mechanism scheme for the heterogeneous Fenton reaction. The comparative spin-trapping EPR experiments on a  $\gamma\text{-Fe}_2\text{O}_3$  nanoparticle catalyst showed that the free radical production should mainly be attributed to the surface iron ions rather than those dissolved metal ions released by the nanoparticles as previously thought. Reprinted with permission from ref. 198 Copyright American Chemical Society 2010.

Beginning in the mid-1990s, researchers started to develop heterogeneous catalysts for Fenton reaction using solid iron-containing compounds as the catalysts.<sup>193-195</sup> The advantages of the heterogeneous systems are obvious: (1) drastically alleviated problem of  $\text{Fe}(\text{OH})_3$  precipitation as little iron ions are present in aqueous phase, (2) easy separation of the catalyst after application; (3) thus broadened pH range where the Fenton reaction can take place.<sup>196, 197</sup> Moreover, Smirnov et al. investigated the free radical generation rate by using spin-trapping electron paramagnetic resonance (EPR) technique and found at least 50-fold more  $\text{OH}^\bullet$  free radicals generated on the iron-oxide surface than by dissolved  $\text{Fe}^{3+}$  in a homogeneous Fenton system (Figure 8 c).<sup>198</sup>

The past decade has experienced great progress in rational design of the nanoparticle based Fenton catalysts (e.g.,  $\text{Fe}_3\text{O}_4$ ,  $\alpha\text{-FeOOH}$ ,  $\alpha\text{-Fe}_2\text{O}_3$ ,  $\gamma\text{-Fe}_2\text{O}_3$ ), assisted by steadily deepening understanding of the Fenton reaction mechanisms. For example, it is known that in a homogeneous Fenton reaction, the  $\text{Fe}^{2+}$  ion produces hydroxyl radicals much faster than  $\text{Fe}^{3+}$  species.<sup>186</sup> Guided by this knowledge, in 2008, Guimaraes et al. applied hydrogen thermal reduction treatment to  $\alpha\text{-FeOOH}$  to induce  $\text{Fe}(\text{II})$  on the material surface, which was found to significantly increase the degradation rate of quinolone.<sup>199</sup> Comparing to other iron containing compounds, magnetite (i.e.,  $\text{Fe}_3\text{O}_4$ ) has recently attracted considerable amount of interests because it is one of the most abundant iron oxide with  $\text{Fe}(\text{II})$  in its crystal structure

and it is still quite stable in air.<sup>200</sup> In addition, the Fe(II) in  $\text{Fe}_3\text{O}_4$  is located in the octahedral sites of the spinel phase crystal and therefore exhibits high surface exposure, which is expected to be an advantage for Fenton reaction. Many published results have proven better performance of magnetite than other iron-containing substances.<sup>200</sup>

In efforts to break the conventional Fenton reaction efficiency limit, many other nano-assisted processes have been rationally combined with the Fenton reaction and resulted in a number of successful Fenton variants (e.g., photo-Fenton reaction,<sup>201-205</sup> electro-Fenton reaction,<sup>206-208</sup> and “Fenton-like” reaction<sup>196, 209, 210</sup>). However, due to the space limitation, these topics are not covered in this review and the interested readers should direct their attention to the AOP or Fenton-focused review articles.<sup>184, 186, 206, 211, 212</sup>

#### 4.2 Nano-assisted $\text{TiO}_2$ based photocatalysis

Photocatalysis-based water treatment processes, much more by oxidization than by reduction, have long been studied. Among all of semiconductor catalysts,  $\text{TiO}_2$  has distinguished itself majorly due to the fact that  $\text{TiO}_2$  is by far the most photostable photocatalyst in aqueous environment.<sup>213</sup> However, its performance under sunlight is limited by two key bottlenecks. The first one comes from its wide band gap nature (3.0 eV for rutile and 3.2 eV for anatase) and thus it is only responsive to ultraviolet (UV) light, which represents only 5% of the total solar spectrum.<sup>19, 214</sup> The second one is its ultra-fast recombination rate of photo-generated electron-hole pairs, which decreases the quantum efficiency.<sup>19, 214, 215</sup> The research efforts to  $\text{TiO}_2$  based water treatment are mainly on overcoming these two bottlenecks in the last two decades.

In an attempt to expanding the  $\text{TiO}_2$  light responsive range, hetero-element doping (e.g., N, F, C) has been widely employed, which is successful in increasing the  $\text{TiO}_2$ 's adsorption of visible light and in making  $\text{TiO}_2$  showing certain level of photocatalytic activity within visible-light range.<sup>19, 216</sup> However, the stability of the hetero-element doped  $\text{TiO}_2$  is generally decreased and its performance under the whole solar spectrum, including UV and visible light, does not usually show a significant improvement in most cases. This is mainly ascribed to that the incorporation of these foreign impurities (e.g., N, F, C) is inevitably accompanied by significantly increased electron-hole recombination centers in the material and thus decreases the quantum efficiency.<sup>19, 216</sup>

Recently, the hetero-element doping strategy has been gradually giving its place to the so-called self-doping by  $\text{Ti}^{3+}$  via various *in situ* reduction methods (e.g.,  $\text{H}_2$  reduction,  $\text{NaBH}_4$ , electrochemical reduction).<sup>217-221</sup> In 2011, Mao et al. demonstrated that reducing the  $\text{TiO}_2$  surface layer by  $\text{H}_2$  treatment could significantly shift the band gap of the  $\text{TiO}_2$  from 3.3 eV in their case to 1.54 eV, which led to the final  $\text{TiO}_2$  product having a black color look (Figure 9a).<sup>222</sup> The black  $\text{TiO}_2$  was proven to be an effective photocatalyst for decomposing organic water pollutants. Recently, many kinds of “colorful”  $\text{TiO}_2$  materials, which indicated their visible light responsiveness, were fabricated by various reduction approaches and their enhanced photocatalytic activities were widely reported.<sup>223, 224</sup> For example, by using aluminum-mediated reduction method, Xie et al. synthesized gray  $\text{TiO}_2$ , which exhibited visible-light and even IR absorption with high photocatalytic activity toward organic pollutant degradation.<sup>225</sup>

In addition to the doping strategy, to rationally engineer the band structure of TiO<sub>2</sub>, TiO<sub>2</sub> hetero-junctions (e.g., P-N junctions, noble-metal-TiO<sub>2</sub> junctions, Schottky junctions) with other visible light photoactive nanomaterials are also a popular option in the same line.<sup>226-228</sup> In 2013, Wang et al. designed and fabricated a gold (Au) nanocrystals-TiO<sub>2</sub> nanotube array nanocomposite material, in which the Au nanocrystals were responsive to the visible light via surface plasmonic resonance (SPR) and injected the photo-generated hot-electrons into the conduction band of the adjacent TiO<sub>2</sub>, thus letting visible light contribute to the photocatalysis reaction (Figure 9b). The shape and size of the Au nanocrystals could be rationally designed and synthesized to engineer their SPR wavelength to make an optimal match with the TiO<sub>2</sub> substrate to maximize the photocatalytic performance of the nanocomposite material.<sup>227</sup> Besides acting as an antenna to capture visible light energy, the second phase material of these hetero-junctions may benefit fast electron-hole separation by design, and thus increase the quantum efficiency. Wang et al. designed a palladium (Pd) and TiO<sub>2</sub> Schottky junction, which considerably reduced the recombination of photogenerated electrons and holes, promoted the electron transfer, and ultimately led to improved performance of photocatalytic oxidation of organic water pollutants.<sup>229</sup>

Because of a general mismatch between optical path length required for light absorption (at least 1 μm for 90% light absorption) and optimal charge diffusion length (usually 70 nm for minority carrier: hole) in TiO<sub>2</sub>, TiO<sub>2</sub> has inherently fast photoelectron-hole recombination in its particle form.<sup>230-232</sup> As it allows for optimization of the optical path length and charge diffusion length relatively independently, one-dimensional nanostructures of TiO<sub>2</sub>, such as nanotubes (NTs), nanorods, and nanowire, are rational solution to the mismatch issue in the TiO<sub>2</sub> particle form.<sup>19, 206</sup> Over the past decade, some reliable and mature synthesis methods for one-dimensional TiO<sub>2</sub> have been developed, including hydrothermal,<sup>233, 234</sup> solvothermal,<sup>235, 236</sup> and anodization.<sup>237, 238</sup> Wang et al. reported a facile two-step anodization method that was able to produce a hierarchical TiO<sub>2</sub> nanotube arrays with a well-controlled surface morphology, which achieved a record-high photoactivity in the category of pure and unmodified TiO<sub>2</sub> material.<sup>215</sup>

High reactive crystal plane is another essential factor for lifting the photocatalytic performance. In 2005, Selloni et al. studied the crystal plane catalytic reactivity through investigation of the methanol adsorption by using density functional theory (DFT) calculation and first principles molecular dynamics (MD) simulations.<sup>239</sup> Their results theoretically proved the high reactivity of TiO<sub>2</sub> {001} crystal plane.<sup>240</sup> However, the unsettling reality is that the {101}, instead of {001}, crystal plane is usually the most dominant one in natural and regular TiO<sub>2</sub> materials. This is so because, comparing with {101} crystal plane whose average surface energy is only 0.44 J/m<sup>2</sup>, the high average surface energy of {001} crystal plane (0.9 J/m<sup>2</sup>) leads it thermodynamically unfavorable, and thus during crystal growing process, the {001} crystal plane diminishes quickly to lower down the total system energy.<sup>241</sup> In 2008, Lu and coworkers first reported uniformly large percentage of {001} crystalline (47%) formation using hydrofluoric acid as morphology control agent<sup>242</sup>. In 2009, Yu et al. reported a microwave-assisted method in synthesizing micro-sheet anatase TiO<sub>2</sub> with 80% level of reactive {001} plane which showed significantly higher 4-chlorophenol degradation performance than the {101} crystal plane dominated TiO<sub>2</sub> (Figure 9c).<sup>241</sup>

Although powder-TiO<sub>2</sub> based photocatalysis has been mainstream in water treatment,<sup>243-245</sup> gaining steam is TiO<sub>2</sub> based photoelectrocatalysis (PEC) in which the photocatalyst is made/deposited on an electrode. Powder TiO<sub>2</sub> generally has higher specific surface area and thus higher level of interaction with the target pollutant in water than the PEC based system. However, the advantages of the PEC based electrode system over the powder-based one should not be underplayed.<sup>41, 246-249</sup> As in a TiO<sub>2</sub> PEC system, the photogenerated electrons go through an external circuit before being ultimately accepted by electron acceptors on the cathode side and, while within the external circuit, an external bias can be applied to vary the energy level of the electrons so to induce some reactions which may not be possible within the TiO<sub>2</sub> powder based system (Figure 9d).<sup>250, 251</sup> One example is that a pure, i.e., unmodified with co-catalyst, TiO<sub>2</sub> powder is not able to reduce water to produce H<sub>2</sub> gas due to the high activation energy barrier of hydrogen evolution even though the TiO<sub>2</sub>'s photoelectron energy level lies negative of the hydrogen evolution level. With a PEC system, an applied external bias can easily make the electrons to jump over the activation energy barrier of the same reaction to split water to generate both H<sub>2</sub> and O<sub>2</sub>.<sup>215, 227, 252-254</sup>

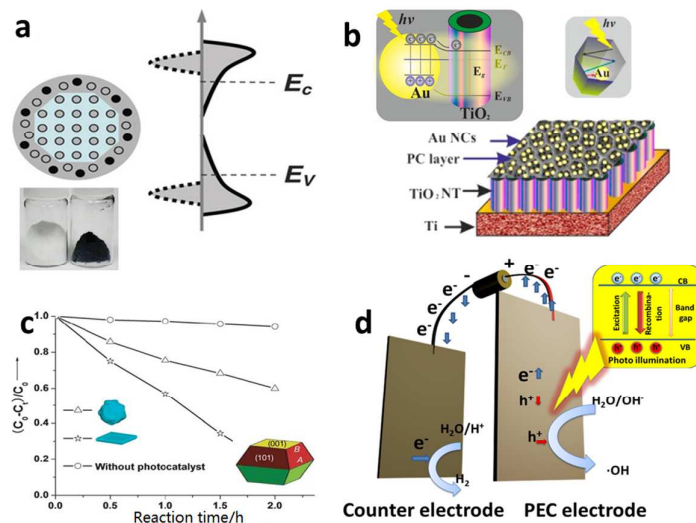


Figure 9 (a) The crystal structure, photo image and electronic density of states (DOS) of the hydrogen reduced black TiO<sub>2</sub>. Its band gap is greatly narrowed because the crystal structure disorder leads to a broadened tails of states extending into the forbidden band gap. Reprinted with permission from ref. 222. Copyright American Association for the Advancement of Science 2011. (b) The structure scheme and energy band structure of plasmonic gold nanocrystals decorated TiO<sub>2</sub> nanotube array. The gold nanocrystals can capture visible light to produce hot electron via SPR process, inject them into TiO<sub>2</sub> nanotube, and thus endow TiO<sub>2</sub> the visible light spectrum response. Reprinted with permission from ref. 227. Copyright American Chemistry Society 2013. (c) A unique TiO<sub>2</sub> single crystal material with controllable exposure of high active {001} crystal planes. The TiO<sub>2</sub> catalyst with higher percentage of {001} planes showed higher catalytic activity in photodecomposition of 4-chlorophenol. Reprinted with permission from ref. 241. Copyright Royal Society of Chemistry 2009. (d) Schematic structural view of a PCE cell, in which an external bias can be applied to the electrode to vary the energy level of the electrons to meet the demand of a

specific reaction.

### 4.3 Nano-assisted reduction processes

Despite the dominance of oxidation processes in water treatment, there are places where reduction-based water treatment is essential. For example, the reductive dechlorination of legacy chlorinated groundwater pollutants, especially TCE, by NZVI is an important process for eliminating the environmental impact of these human carcinogens from water resources. The NZVI in the reaction acts as reductant.<sup>56-63, 255-257</sup>

Given the high water solubility and low adsorptive capacity of such water pollutants as oxyanions (e.g.,  $\text{NO}_3^-$ ,  $\text{ClO}_4^-$ ,  $\text{BO}_3^-$ ), nitrosamines, and PPCPs, etc., conventional water treatment approaches suffer from their own limitations. Development of high efficient heterogeneous chemical catalysts for the reduction of these compounds becomes a more popular strategy nowadays.<sup>258</sup> Nanoscale Pd based catalysts possess high activities in lots of reduction reactions and have found wide applications in reductive transformation of many water pollutants. In the mid 1990s, Abu-Omar and Espenson found that a rhenium(V) complex could serve as an efficient catalyst for the reduction of perchlorate to chlorate, using hypophosphorous acid ( $\text{H}_3\text{PO}_2$ ) as a reducing agent.<sup>239,259</sup> Although their method has been continuously improved,<sup>260</sup> such a homogeneous catalysis system with soluble reducing agents is not suitable for water purification systems. In 2007, Shapley et al. developed the first oxorhenium (VII)-based heterogeneous catalyst for perchlorate reduction using carbon as support along with Pd metal particles (Re-Pd/C),<sup>261</sup> which promoted the complete reduction of perchlorate to chloride by using hydrogen as the reducing agent under an condition of  $\text{pH} < 3$ . In 2009, Shapley et al. further reported that the presence of substituted pyridine ligands was able to greatly improve the activity and stability of this Re-Pd/C catalyst.<sup>262</sup> However, in this system, rhenium species were immobilized in the activated carbon support only by electrostatic interactions, which led to rhenium leaching problem.<sup>263</sup> In 2013, Choi et al. reported a Pd on N-doped activated carbon (Pd/N-AC) system for perchlorate reduction, in which the N-doped carbon surface provided adsorption sites for perchlorate due to the basic nitrogen functional groups on the surface and the supported Pd clusters acted as the catalyst for the perchlorate reduction in hydrogen atmosphere (Figure 10a).<sup>264</sup> The adsorption of perchlorate on this N-doped carbon support (3.67 mg/g) was believed to be a key process for this method. However, the low adsorption capacity and low ion selectivity of the activated carbon necessitate frequent regeneration of the adsorbents. In 2014, Strathmann and Werth along with coworkers designed an ultra-small Pd clusters (< 2nm) within ion-exchange resin as an adsorption/catalysis bi-functional material for perchlorate reduction. In this system, a  $\text{ClO}_4^-$  selective ion-exchange resin was adopted to replace activated carbon support for its high adsorption capacity (~ 200 mg/g) and selectivity, which significantly improved the  $\text{ClO}_4^-$  reduction efficiency and the catalyst reusability.<sup>265</sup>

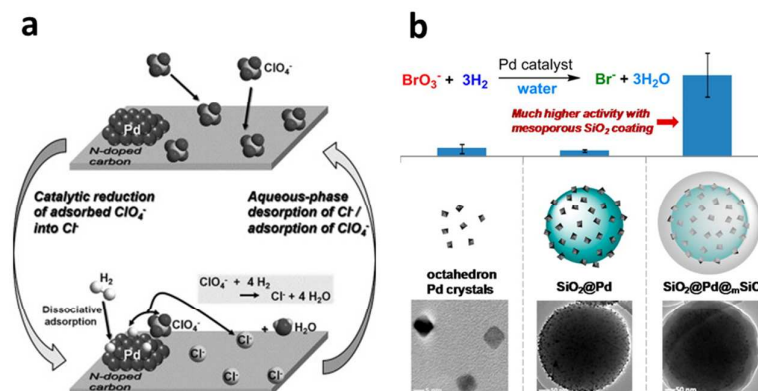


Figure 10 (a) The perchlorate adsorption-reduction cycle on a Pd/N-doped activated carbon (Pd/N-AC) catalyst. The N-doped carbon provides ample adsorption sites for perchlorate and thus benefits the subsequent catalytic reduction by Pd clusters in hydrogen atmosphere. Reprinted with permission from ref. 264. Copyright Elsevier Inc. 2013. (b) A core-shell structured catalyst, composed of a Pd-nanoparticles-decorated  $\text{SiO}_2$  nanosphere core and a mesoporous silica shell, exhibits much higher activity in the reduction of bromate. Reprinted with permission from ref. 69. Copyright American Chemical Society 2014.

Furthermore, In 2011, Reinhard et al. used bimetallic palladium–indium (Pd–In) nanoparticles supported on alumina for the reduction of *N*-nitrosodimethylamine (NDMA) and found that indium served as a promoter metal.<sup>266</sup> In 2013, Werth et al. examined the activity of Pd nanoparticles in catalytic reduction of nitrite ( $\text{NO}_2^-$ ), NDMA, and diatrizoate as a function of Pd crystal plane.<sup>267</sup> However, the ultra-small size of Pd nanoparticles is not conducive to their practical applications due to the particle aggregation problem and the difficulty in catalyst separation and recovery. In 2014, Strathmann and Werth, along with coworkers, reported a core-shell-structured catalyst with encapsulated Pd nanoparticles for the reduction of bromate ( $\text{BrO}_3^-$ ) using  $\text{H}_2$  as reducing agent at room temperature.<sup>69</sup> The Pd nanoparticles with 6 nm size were firstly decorated on the surface of the solid silica nanospheres, which were then further encapsulated with an ordered mesoporous silica shell with 2.3 nm pore size. The mesoporous shell provided a physical barrier to prevent Pd from leaching and aggregation and at the same time it, due to its ordered porous structure, ensured the accessibility of the Pd nanoparticles by the reactants. It was, although surprising, quite interesting that the mesoporous silica shell could promote  $\text{BrO}_3^-$  adsorption near the Pd active sites and thus greatly enhanced the catalytic activity by a factor of 10, comparing to the otherwise same catalyst without the mesoporous silica shell (Figure 10b). The dual functions of the mesoporous shell, enhancing the Pd catalyst activity and preventing aggregation of the active nanoparticles, suggest a general and promising strategy of using metal nanoparticle catalysts for water treatment and or other relevant aqueous-phase applications.

## 5. Rational design of nano-assisted membrane based separation

Over the past decade, nanomaterials have set foot in almost all areas of conventional membrane based separations, including microfiltration (MF), nanofiltration (NF), ultrafiltration (UF), membrane distillation (MD), forward osmosis (FO) and reverse osmosis (RO), and many nano-assisted membrane processes have recorded significant progresses.<sup>11, 268-278</sup> This section discusses the rational design of nano-assisted membrane processes by focusing majorly on RO and FO, along with discussions on emerging next-generation inorganic membranes and active membrane filtration.

### 5.1 Nano-assisted RO and FO performance enhancement

Generally, the modern FO and RO membranes share commonality in structural configuration, both consisting of a thin dense active layer, supported on a thick microporous support layer.<sup>270, 271, 279-281</sup> The support layer does not contribute to the salt rejection and it is the active layer where the separation occurs. The dense active layer backbone material in the modern RO and FO membranes is dominated by polyamide due to its high salt rejection.<sup>271, 279, 281, 282</sup> The major concern in RO nowadays is with its energy consumption caused by high operation pressure, which is in turn forced by the desire of high water flux.<sup>270, 272, 274</sup> Consequently, the research efforts in nano-assisted RO membrane have been focused majorly on increasing water flux by blending selected nanomaterials (e.g., zeolite, silica nanoparticles, CNTs, aquaporin protein) in polyamide-based active layers.<sup>283-287</sup> The essence of the nanomaterial blending strategy lies in the preferential water channels created by placing the selected nanomaterials in a polyamide matrix.<sup>11, 272</sup>

Inspired by the superior molecular sieving effect in zeolite, in 2007, Hoek et al. fabricated a zeolite blended polyamide active layer on top of a polysulfone support (Figure 11a), which exhibited a water flux two times that of non-modified membrane under an optimized zeolite particle loading without decreasing the salt rejection rate.<sup>286</sup> In 2001, Hummer et al. reported a MD simulation result that showed water molecules were able to rapidly move through carbon nanotubes with a pulse-like transmission behavior<sup>288</sup> and in 2003, their MD simulation result further showed that water molecules may flow through membranes of open-ended CNTs under an osmotic gradient in an almost friction-less manner and the resulted water flow rate was comparable to those measured for biological water channels, such as aquaporin.<sup>289</sup> In 2011, Zhang et al. synthesized a functionalized multi-walled carbon nanotubes (MWCNTs) incorporated polyamide-based active layer in a RO membrane, which exhibited a significantly increased water flux, from 26 L/m<sup>2</sup> h (LMH) with the original membrane to 71 LMH with the MWCNTs blended membrane.<sup>290</sup> Due to the hydrophilicity and thermal stability of silica, in 2008, Singh et al. blended silica nanoparticles (16 nm and 3 nm) into polyamide active layer in a RO membrane and reported a water flux increase of 200% with the same level of salt rejection under an optimal nanoparticle loading (21.3 vs. 9.0 LMH with and without the silica blending).<sup>291</sup> Later, Deng et al. incorporated mesoporous silica MCM-41 into polyamide active layer and recorded a water flux of 46.6 LMH in comparison to 28.5 LMH without MCM-41. They suggested that the internal pores of MCM-41 contributed significantly to the increase of water permeability.<sup>292</sup>

Biological membrane evolves effective way for water transportation via aquaporin proteins and this has been inspirational to RO and FO membrane modification.<sup>272, 293</sup> In 2007, Zilles and Clark et al. fabricated amphiphilic triblock-polymer vesicles containing aquaporin Z, which showed a complete salt rejection and water productivity 800 times that of pure polymer without aquaporin Z.<sup>294</sup> Recently, Tang et al. directly incorporated aquaporin Z into the active layer of a RO membrane via the interfacial polymerization method and the prepared membrane exhibited water permeability an order of magnitude higher than a typical seawater RO membrane.<sup>295</sup>

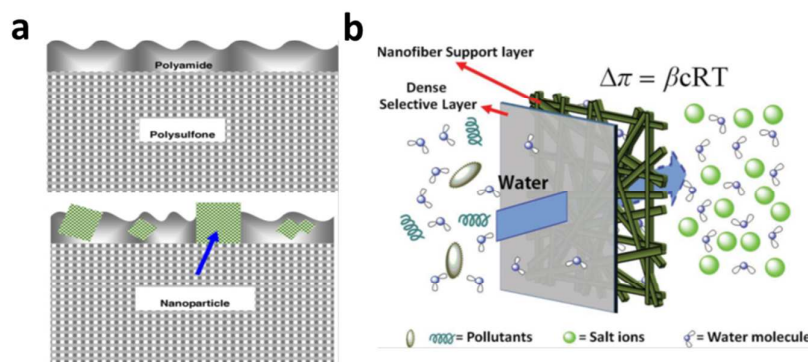


Figure 11 (a) Schematic of a typical RO or FO membrane configuration, with a top thin dense active layer (made of polyamide) supported on a thick microporous support layer (made of polysulfone) (top figure) and the membrane with zeolite nanoparticles blended in the top thin active layer (bottom figure). From ref 286 Copyright © 2007 Elsevier B.V. All rights reserved. (b) Schematic of an FO membrane, with a thin dense active layer and a highly porous support layer made of electrospun fibers to alleviate the adverse effect from ICP. From ref 302 Copyright © 2007 American Institute of Chemical Engineers (AIChE).

Concentration polarization is a serious issue in both RO and FO, which causes a significant decrease in water flux and therefore in operation efficiency.<sup>296-298</sup> FO relies on natural osmotic pressure to drive water selectively through a FO membrane and internal concentration polarization (ICP) is a phenomenon in which the water permeating through porous support layer concentrates/dilutes the salts inside the porous support layer. The ICP leads to reduced osmotic pressure in FO and thus is very problematic as it would cost a drastic loss of driving force in the process.<sup>299, 300</sup> In early times when RO membranes were directly taken for FO processes, more than 90% of the driving force was lost due to the ICP problem. Even with the latest progress in FO membrane fabrication, ICP still cost more than 50% of the driving force.<sup>296, 301</sup> Therefore, at this point, in FO membrane, it is not the active layer, but the support layer that is the bottleneck of the FO process. As expected, nano-assisted and rationally engineered FO support layer has been making its contribution in reducing the adverse effect of ICP.

From the rational design point of view, it has been proposed that an ideal FO support layer should have large porosity, thin layer structure and low tortuosity, and at the same time it should provide enough mechanical strength to support the active layer.<sup>302, 303</sup> Following this

idea, in 2011, Sun et al. fabricated a FO membrane with the support layer made of electrospun nanofibers (Figure 11b), which showed a water flux 3.5 times that of a commercial FO membrane tested under the otherwise same conditions.<sup>302</sup> Tang et al. proposed that incorporation of porous nanomaterials in FO support layer would alleviate the adverse ICP effect, and they demonstrated the effectiveness of this proposal by blending zeolite and nanoporous silica gels into polysulfone support layers.<sup>274</sup> Their results showed that with these rationally selected nanoparticles in the support layers, a significantly improved water flux (2.5 times) was obtained comparing with the original unmodified FO membrane, and their work identified an optimal 10 nm pore size of silica gel for the best FO performance.

## 5.2 Nano-assisted RO and FO anti-fouling

Membrane fouling occurs when suspended solids, microbes, and organic materials deposit on the surface of RO and FO membranes.<sup>304-307</sup> Membrane fouling significantly decreases membrane lifespan and increases operation costs, but is seemingly an inevitable byproduct of selective water permeation in RO and FO membrane. With the recent progresses in RO and FO water flux enhancement, the research effort in the membrane anti-fouling becomes more and more pressing as membrane fouling worsens along with increasing water flux. Two common strategies toward membrane anti-fouling are developed which can be described as (1) anti-adhesion modification and <sup>308-310</sup>(2) anti-microbial modification.<sup>306, 311, 312</sup>

The majority of research activities in the anti-adhesion modification front focuses on surface hydrophilic modification in light of the fact that most of membrane foulants, such as protein, bacteria, large organic compounds, are largely hydrophobic,<sup>313</sup> which was first uncovered by Belfort et al. in 1997.<sup>314</sup> With a hydrophilic surface modified RO or FO membrane, a thin water layer would form on the membrane surface, preventing the hydrophobic fouling substances from adhering onto the membrane. Based on this idea, in 2007, Cao et al. reported a method for surface grafting poly(ethylene glycol) (PEG) layer during the active layer fabrication, and the PEG grafted RO membrane showed an improved antifouling performance.<sup>315</sup> Takahara et al. modified membrane surfaces with several polymer brushes with different surface tension to investigate the relationship between surface wettability and their antifouling behaviors and their results proved that the hydrophilic surface had much better antifouling property towards hydrophobic foulants than the hydrophobic ones.<sup>316</sup>

Given the ubiquitous presence of microorganism, microorganism, especially bacteria-induced fouling is not uncommon in many RO and FO membranes and therefore biocide-induced anti-biofouling strategy is a rational solution in these cases.<sup>11, 276, 313</sup> The many-century old knowledge of the antimicrobial property of silver metal has led scientists to use silver, especially silver nanoparticles, for the antifouling purpose due to their high antibacterial activity and simple synthesis. In 2009, Yang et al. prepared silver nanoparticle-coated commercial polyamide RO membrane and tested its anti-biofouling properties in seawater desalination process. Their results showed an obvious decrease in the microbial concentration on the membrane surface.<sup>317</sup> In 2014, Elimelech et al. modified polyamide RO membrane with silver nanoparticles via layer-by-layer (LbL) assembly, followed by further modification with a polymer brush of poly(sulfobetaine) or PDMS. All modified membrane surfaces exhibited significant reduction of irreversible bacterial cell adhesion as

well as strong anti-bacterial activity (Figure 12).<sup>318</sup>

In 2007, Elimelech et al. first reported antibacterial activity of single walled CNTs (SWCNTs),<sup>319</sup> and in 2012 the same group prepared an antimicrobial film through Lbl assembly of SWCNTs with polypeptides.<sup>320</sup> In 2013, it was further revealed that bundled SWCNTs had much fast bacteria inactivation kinetics than unbundled ones.<sup>321</sup> In 2014, it was found that graphene oxide (GO) possessed a broad spectrum of antimicrobial activities.<sup>322</sup> Very recently, Elimelech's group investigated the GO's antimicrobial activity as a function of its size<sup>323</sup> and showed that the GO's antimicrobial activity increased sharply as its size decreased due to the higher defect density of smaller GO sheets. The same group prepared a GO nanosheet modified polyamide active layer on a RO membrane via surface amide coupling and reported high level and fast antibacterial activity on the membrane.<sup>324</sup>

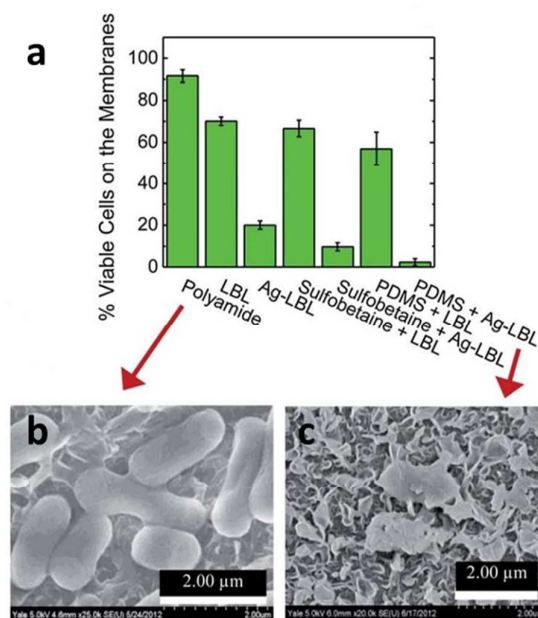


Figure 12 (a) The histogram of residual live cells (*E. coli* K12) on different modified membranes through live/dead assay. The SEM images of the cells on the surface of (b) polyamide and (c) PDMS/Ag modified membranes, respectively, which represented the worst and best antibacterial performance among these materials. Reprinted with permission from ref. 318 Copyright Royal Society of Chemistry 2014.

### 5.3 Emerging next-generation membranes

Unbounded by the currently available membranes, the development of nanomaterials in the past 10 years, constantly aided by MD simulation as a designing guide, has led to many brand-new membranes, especially inorganic membranes, that are completely out of the limits of conventional membrane materials.<sup>288, 289, 325-328</sup> The recent developments in this regard include membranes wholly made of CNTs,<sup>329</sup> graphene,<sup>330</sup> graphene-oxide (GO),<sup>331</sup> and reduced graphene-oxide (rGO),<sup>332</sup> etc. Among them, graphene, inclusive of GO and rGO, based membranes have shown unprecedented performances and thus represented a very promising direction in next-generation water treatment, especially in nanofiltration and

seawater RO desalination, which will be the focus of the next paragraph.

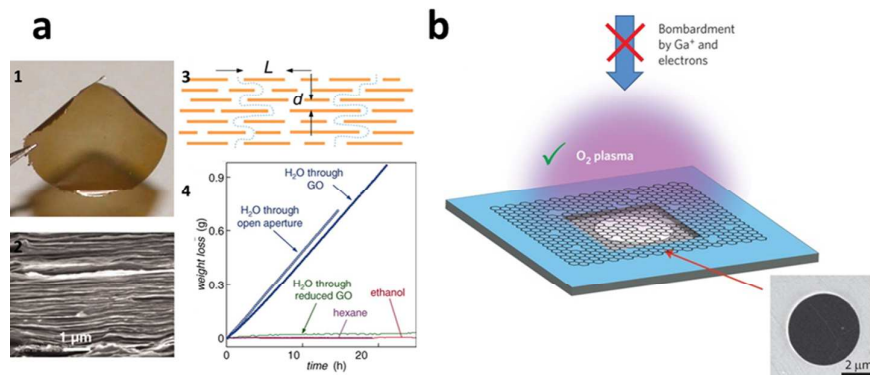


Figure 13 (a) (1) The optical and (2) SEM image of a 1 μm-thick GO membrane prepared by spin coating method; (3) a possible penetration mechanism through the GO membrane; (4) the permeation rates results showed that the ethanol and hexane were impermeable while water could quickly pass through the membrane. Reprinted with permission from ref. 331. Copyright American Association for the Advancement of Science 2012. (b) Ultra-small nanoholes were fabricated on a single layered graphene membrane supported by a copper foil via O<sub>2</sub> plasma treatment, which showed much better performance in water desalination than those treated by electrons or gallium ions. Reprinted with permission from ref. 330. Copyright Nature Publishing Group 2015.

In 2010, using MD simulation, Aluru and coworkers first investigated and compared the water penetration process within graphene membrane,<sup>327</sup> and pointed out the potential of graphene-based membrane for water filtration. In 2012, a detailed MD study by Grossman and Cohen-Tanugi revealed that nanometer-scale pores in single-layer freestanding graphene could effectively filter out NaCl salt from water and they predicted that its water permeability would be several orders of magnitude higher than conventional RO membranes.<sup>326</sup> In the same year, Geim, the 2010 Noble Prize laureate for his work with graphene, and collaborators prepared a semimicrometer-thick GO membrane by spin coating and their permeation experiments showed that the GO membrane was impermeable to the tested liquids, gases and vapors, but allowed unimpeded permeation of water with a flow rate 10 orders of magnitude faster than Helium (Figure 13 a).<sup>331</sup> In 2014, Geim et al. further synthesized a 5.0 μm thick GO membrane by simple vacuum filtration method and found that the GO membrane, if immersed in water, acted as molecular sieves, blocking all solutes with hydrated radii larger than 4.5 angstroms. And more interestingly, it was found that smaller ions permeated through the membranes at rates thousands of times faster than what is expected for simple diffusion.<sup>101</sup> They contributed the anomalously fast permeation of the small ions to a capillary-like high pressure acting on ions inside graphene interlayer spaces. The fact that the major seawater ionic species, including Na<sup>+</sup>, K<sup>+</sup>, Mg<sup>2+</sup>, Cl<sup>-</sup>, can easily permeate through the GO membrane makes it impossible for RO and FO applications for water desalination. However, the ultrafast ion transport and precise molecular sieving size cutoff promises the GO membrane a lot of applications in nanofiltration category. In 2014, Park et al. synthesized a double-layered graphene membrane and perforated it with focused

ion beam milling to produce plenty of pores ranging from 10 nm and 1 micrometer and the perforated graphene membrane showed water permeation far in excess of those shown by finite-thickness membranes.<sup>333</sup> In 2015, a single layered graphene membrane with nanoscale pores were created by a team from Oak Ridge National Laboratory using plasma etching process (Figure 13b) and the resulted membrane exhibited a salt (e.g., LiCl, NaCl, KCl) rejection rate of nearly 100% and rapid water transport, making it a promising next-generation RO and FO membrane for water desaliantion.<sup>330</sup> Other interesting work include: using the same vacuum filtration followed by HI reduction, Zhang et al. synthesized a freestanding ultrathin (lower than 20 nm) rGO membrane, which showed an outstanding performance as a FO membrane.<sup>332</sup> Mi et al. prepared GO membrane via LbL assembly and subsequent crosslinking and the membrane showed water flux 4–10 times higher than most commercial NF membranes.<sup>334</sup> Mxenes, due to their atomic layered structures similar to graphene-based materials, highly controllable chemical composition, high aspect ratio, promises a bright prospective in membrane-based filtration, but unfortunately there hasn't been any published result on this thus far.

#### 5.4 Active filtration membranes

In comparison to the traditional concept of membranes being physical and permeable barriers for physical separation of two bulk phases, such as in RO and FO processes, arising is a trend where adsorption and/or more importantly chemical processes (e.g., catalysis, reduction, oxidization) are being combined with membrane filtration to achieve active filtrations for more energy-efficient water treatment.<sup>335-340</sup> When operated under pressure-driven convective flow, the active membranes provide reactants rapid access to active sites, thereby minimizing the mass transfer limitations associated with other high surface area-to-volume materials, leading to enhanced treatment performance.<sup>337</sup> Examples of the active filtration membranes include: TiO<sub>2</sub> or other semiconductor-based photo(electrochemical)-catalytically active membrane filters,<sup>338</sup> CNT-based electrochemically active filters,<sup>136</sup> noble-metal (e.g., Au, Pd) based catalytically active membrane filters,<sup>336</sup> Fenton-reaction reactive membrane filters, etc.<sup>337,341</sup> In a typical electrochemically or photoelectrochemically active membrane filtration system, the membrane serves as a working electrode (either cathode or anode depending on the targeted reactions) which is connected to a counter electrode to provide the required potential. Therefore, it is required that the membrane material has to be or be made electro-conductive.<sup>136</sup> Among suitable candidate materials, CNT-based electrochemically active filters have been studied intensively. For instances, CNT-based electrochemically active filters have been demonstrated effective in removing aqueous organic pollutants, such as salt, proteins, viruses, azo dyes, PPCPs, perfluorinated chemicals, and phenol.<sup>137, 342-349</sup> However, the potential of other conductive materials, especially graphene, rGO, Mxenes, conductive polymers in this regards should not be underestimated.

## 6. Rational design of superwetting surfaces for oil-water separation

With fossil fuel, especially gasoline and diesel, being a dominant energy source in personal transportation, deliberate and accidental release of oil into aqueous environment takes place

in every step of the lifecycle of petroleum and is nowadays a serious environmental concern. Efficient oil-water separation technologies are highly sought after as environmental response measures. The conventional oil-water separation technologies, such as physical skimmer, hydrocyclone-based separation, membrane-based separation, generally involve external energy sources to drive separation.<sup>350-352</sup> Recently, rapid development of interface science along with bionics has helped in evolving a brand-new concept of using superwetting materials,<sup>353, 354</sup> generally in the form of two-dimensional membranes, for the oil-water separation in the absence of external energy input.<sup>350-352, 355-361</sup> The superwetting capability of materials, which is a result of a proper combination of their surface micro-nano hierarchical structure and surface chemistry, refers to such extreme wetting behaviors as superhydrophobicity, superhydrophilicity, superoleophobicity, superoleophilicity, superamphiphilicity, and superamphiphobicity. The inspirations of the superwetting materials usually have their roots in nature and the bio-inspired materials with superwetting capability have shown tremendous advantages over conventional methods in the field of oil-water separation as they allow for gravity-driven separation.

In 2002, Jiang et al. revealed that a combination of spatial micro- and nanometer-scale hierarchical surface structures and proper chemical composition resulted in the superhydrophobic self-cleaning effect of lotus leaf,<sup>362</sup> which led them to develop the first example of superwetting (superhydrophobic/superoleophilic in their case) membrane for the oil-water separation in 2004.<sup>363</sup> In their work, a low-surface-energy material of polytetrafluoroethylene (PTFE) coated stainless steel mesh, which had a water contact angle greater than 150° and a diesel contact angle of ~ 0°, was used to effectively separate oil from water.

Later, researchers came to realize that because the superhydrophobic and superoleophilic materials removed only oil, this oil-removing type of materials could be easily fouled or even blocked by oils because of their intrinsic oleophilic property, which seriously impact the lifetime of the materials.<sup>350-352</sup> In addition, the oil adhered or adsorbed on the materials is hard to be removed, resulting in a secondary pollution during the post-treatment process.<sup>350-352</sup> In an effort to solve this problem, Jiang and coworkers, inspired by the oil-repellent capability of fish scale (Figure 14a),<sup>364</sup> recently fabricated a novel superhydrophilic and underwater superoleophobic hydrogel coated mesh for oil-water mixture separation (Figure 14b).<sup>365</sup> This water-removing type of materials has completely opposite wettability to traditional hydrophobic and oleophilic materials and thus overcomes propensity to fouling and recycle problems because they (1) selectively allow water, instead of oil, to pass and thus prevent oil to make contact with the materials, which effectively avoids or reduces the possibility of membrane clogging caused by viscous oil phase; (2) allow for a true gravity-driven separation of oil/water phases due to the fact that water is generally heavier than oil phase (Figure 14).<sup>366, 367</sup> Similarly, Jin and coworkers recently reported the fabrication of a novel poly-(acrylic acid)-grafted PVDF filtration membrane using a salt-induced phase-inversion approach. A hierarchical micro/nanoscale structure was constructed on the membrane surface, which endowed the membrane with a superhydrophilic and underwater superoleophobic property and thus allowed for effective separation of oil-in-water emulsions.<sup>368</sup>

Although (super)hydrophilic and underwater superoleophobic membranes are effective for the separation of oil-water mixture, in practical applications, the hydrophilic or superhydrophilic surfaces of the separation materials are still prone to contamination by low-surface-energy substances presented in the mixture due to their intrinsically high surface energy.<sup>369, 370</sup> These low-surface-energy contaminants, once adsorbed, are difficult to remove and often deteriorate the surface wetting behaviors, and thus degrade the separation performance. It is for this reason that frequent washing-based maintenance for the separation membranes is indispensable, which adds to the high operational cost of the separation. To this end, Wang et al. reported a self-cleaning underwater superoleophobic mesh for oil-water separation, which was prepared by LbL assembly of sodium silicate and TiO<sub>2</sub> nanoparticles on stainless steel mesh.<sup>371</sup> Compared with organic separation membrane, which suffers from poor stability and may become unstable under harsh conditions, the all-inorganic silicate/TiO<sub>2</sub> coating provided improved stability. Furthermore, the integration of the self-cleaning property of TiO<sub>2</sub> into the all-inorganic separation mesh enables a convenient removal of the fouling contaminants by ultraviolet (UV) illumination, and allows for an easy recovery of the separation ability of the mesh once contaminated (Figure 14c).

In view of the diversity of oil-water mixtures and complexity of oil-spill incidents, a controllable oil-water separation is highly desirable, i.e., the separation material allows either oil or water to pass through on demand.<sup>372-377</sup> Wang et al. for the first time demonstrated a smart surface with switchable superoleophilicity and superoleophobicity in aqueous media for controllable oil-water separation<sup>372</sup> as illustrated in Figure 14d and 14e. This surface is the first one of its kind that can switch its superoleophilicity and superoleophobicity under room temperature and without any organic solvent involved. To obtain a smart surface with switchable oil wettability in aqueous media, especially between superoleophobicity and superoleophilicity, the chemistry on the surface should be delicately designed such that it comprises both hydrophilic and oleophilic/hydrophobic characteristics, with either characteristic becoming dominantly exposed over the other in response to environmental conditions. In this work, they grafted a block copolymer comprising pH-responsive poly(2-vinylpyridine) and oleophilic/hydrophobic polydimethylsiloxane blocks (i.e., P2VP-b-PDMS) to functionalize inexpensive and easily available materials, including non-woven textiles and polyurethane sponges and the functionalized materials possessed switchable superoleophilicity and superoleophobicity in aqueous media (Figure 14d), which was highly efficient in controllable oil-water separation. The P2VP block on the grafted block copolymer can alter its wettability and its conformation via protonation and deprotonation in response to the pH of the aqueous media, which in turn provides controllable and switchable access of oil by the oleophilic PDMS block on the surface (Figure 14e).

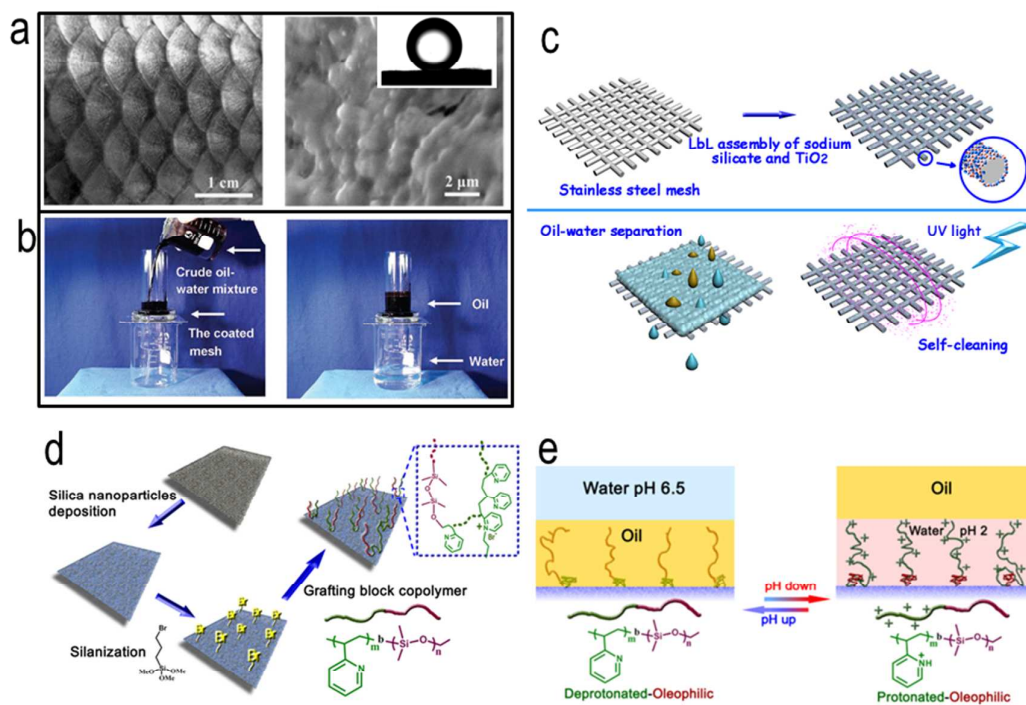


**Figure 14.** (a) Surface structures of fish scale. Inset in (a): shape of an oil droplet on fish scales in water, showing the superoleophobicity of the fish scales. Reprinted with permission from ref. 364. Copyright WILEY-VCH Verlag GmbH & Co. KGaA, Weinheim 2009. (b) Oil/water separation by the hydrogel-coated mesh. The coated mesh was fixed between two glass tubes and the mixture of crude oil and water was put into the upper glass tube. Water selectively permeated through the coated mesh, while the oil was repelled and remained in the upper glass tube. Reprinted with permission from ref. 365. Copyright WILEY-VCH Verlag GmbH & Co. KGaA, Weinheim 2011. (c) Scheme for the preparation of the self-cleaning underwater superoleophobic mesh for oil-water separation. Reprinted with permission from ref. 371. Copyright Nature Publishing Group 2013. (d) Preparation and characterization of a surface with switchable superoleophilicity and superoleophobicity on a non-woven textile substrate. (e) Switch of wettability between underwater superoleophilicity and superoleophobicity. Reprinted with permission from ref. 372. Copyright Nature Publishing Group 2012.

## 7. Multifunctional all-in-one nanomaterials and nanodevices for designed purposes

Given the inherent complexity of natural water and quite contrasting application scenarios in reality, an ideal design of nanomaterial for water treatment is expected to be proactively complex, necessitating multi-functions on individual nanomaterials working hand-in-hand to achieve a designed goal. In the past few years, some enlightening synergistically multi-functional all-in-one nanomaterials and in many cases, integrated nano-devices, have been proposed, prepared and successfully tested, many of which represent

proof-of-concepts of some ground-breaking and next-generation concepts in water treatment and more broadly in clean water production. Followings are three examples we selected among many interesting and inspirational ones.

**An all-in-one, on-demand Fenton-active filtration device.** In 2007, Bhattacharyya et al. rationally designed and fabricated an all-in-one Fenton-reaction-active filtration system for advanced oxidation toward water treatment applications, integrating of nanostructured materials, enzymatic catalysis, and iron-catalyzed free radical reactions within pore-functionalized synthetic membrane platforms (Figure 15a).<sup>337</sup> In this work, within a two-layered membrane, glucose oxidase was immobilized in the top membrane layer to *in situ* generate  $H_2O_2$  by reacting with deliberately added glucose in the raw water, which allowed for the flexibility of on-demand initiation of the Fenton reaction. And, once the  $H_2O_2$  was generated, it was flushed down to the second membrane layer where it reacted with the polymer-immobilized  $Fe^{2+}/Fe^{3+}$  or iron oxide nanoparticles to kick off Fenton reaction for the oxidation of pollutants in the raw water within the confined membrane pore space. The rational design of this active filtration system represents a great stride in on-demand initiating chemical reaction and moving the chemical reaction within confined spaces for breaking the conventional reaction efficiency limit.

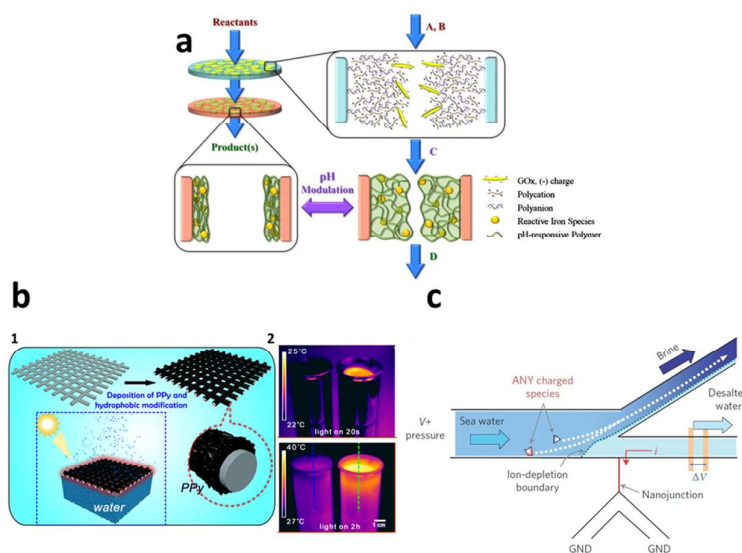


Figure 15 (a) Schematic of a Fenton reactive membrane-based filtration system with a stacked configuration. The bioactive (top) membrane contains immobilized enzyme for the catalytic production  $H_2O_2$  from glucose. The bottom membrane contains either immobilized iron ions or ferrihydrite/iron oxide nanoparticles for the decomposition of hydrogen peroxide to form powerful free radical oxidants for AOP.<sup>337</sup> Reprinted with permission from ref. 337. Copyright National Academy of Sciences, USA 2011. (b) (1) The fabrication process of a solar-light-to-heat conversion membrane by coating a polypyrrole layer on a stainless steel mesh followed by fluoroalkylsilane modification. (2) The infrared (IR) thermal images demonstrated a high efficiency of the interfacial heating produced by the fabricated membrane under solar illumination. Reprinted with permission from ref. 384. Copyright WILEY-VCH Verlag GmbH & Co. KGaA, Weinheim 2015. (c) Schematic of the

micro/nanofluidic desalination system designed by utilizing the ion concentration polarization effect, which involves using bifurcated channels to separate desalted and salted streams and is able to obtain continuous desalination flow. Reprinted with permission from ref. 385. Copyright Nature Publishing Group 2011.

**An all-in-one, self-floating and self-healing solar-driven desalination device.** Solar evaporation is an important approach for massive production of clean water. However, the conventional solar evaporation experiences high level of energy loss and thus low evaporation rate due to its bulk water heating nature.<sup>378, 379</sup> Recently, inorganic photothermal nanomaterial, especially carbon black, CNTs, gold nanoparticles,<sup>380-383</sup> based heating becomes a promising strategy to improve the energy efficiency of solar-driven water evaporation. In 2015, Wang et al. rationally designed and fabricated an interfacial heating membrane, which spontaneously stayed at the water-air interface due to its hydrophobicity, collected and converted solar light into heat with high efficiency, and locally heated only the water near the air/water interface.<sup>384</sup> In this work, polypyrrole (PPy) was chosen as the polymeric photothermal material because of its high adsorption of solar light, photostability, and easy processing, and it was coated on the surface of stainless steel by electropolymerization. The PPy-coated mesh was modified to be hydrophobic with a Wenzel's wetting behavior for high heating efficiency (Figure 15b). The rationally designed membrane possessed significantly enhanced water evaporation rate, with a solar energy to heat conversion efficiency being 58% in comparison to natural solar bulk heating efficiency of only 24%. Moreover, given the likelihood of losing its hydrophobicity caused by UV radiation during applications, the photothermal mesh in this work was made capable of recovering its hydrophobicity once lost. Based on this concept, an all-in-one and point-of-use solar desalination device was fabricated and could produce ca. 750 g/m<sup>2</sup> fresh water from seawater or wastewater under 5 hour natural solar irradiation.<sup>384</sup>

**An all-in-one, point-of-use water desalination cell.** In 2010, Han et al. employed the concept of ion concentration polarization within nanofluidics channels and created an external pressure free, fouling-free, all-in-one direct seawater desalination device<sup>385</sup> (Figure 15c). In this device, a continuous seawater flow was divided into desalted and concentrated flows by ion concentration polarization effect. Since the salts and larger particles were pushed away from the channels during the permeation, the possibility of membrane fouling and salt accumulation were both greatly reduced. Although the electrical efficiency was miscalculated in the original paper,<sup>386</sup> the unconventional desalination concept from this work is enlightening and represents a great effort in next generation desalination technologies, especially in the point-of-use front.

It is generally true that the complexity in the synergistically multi-functionalized nanomaterial design and subsequently synthesis is paid off in the application stage as these nanomaterials lessens the requirements for applications or even open new applications impossible with conventional water treatment systems.

## 8. Concluding remarks

From the discussion throughout this review, one can see that the rational design emphasizes 'design-for-purpose'. Unlike the trial-and-error approach, on the basis of deep understanding of water treatment process, a rational design process always starts with scientifically, generally chemically, defining the problem to be solved in details, such as what the barrier is, what the key to the solution is, the problem can only be solved only if one condition is met, etc. Based on the clear problem definition, a conceptual design of nanomaterial-based solution is proposed, which is then fed back to the problem definition to be scientifically tested. The communication is iterated until both the problem definition and nanomaterial design agree well with each other. Next, the conceptually designed nanomaterial, which just passes the scientific check, is checked with the currently available synthesis capability and then be synthesized if passing. Otherwise, the iteration back to the nanomaterial design will take place until the designed nanomaterial can be successfully synthesized. The performance of the synthesized nanomaterial is then assessed toward its designed purpose which has been unambiguously defined in the problem definition step, and the iteration back to the nanomaterial design will take place again in the event of an unsatisfactory performance of the nanomaterial (Figure 16 b).

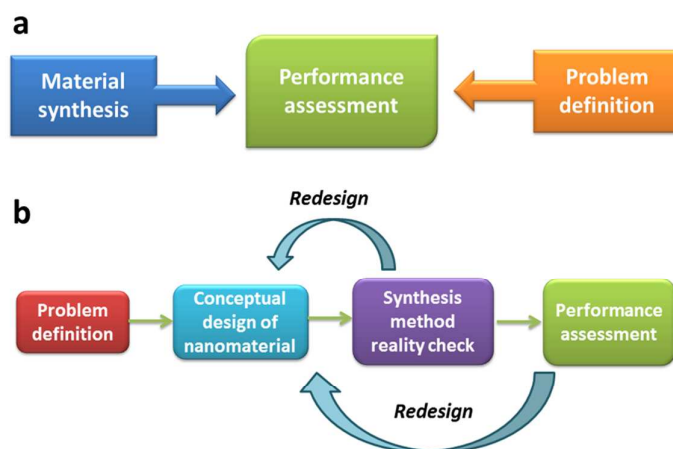


Figure 16 (a) trial-and-error approach versus (b) rational design of nanomaterials for purpose

Rational design involves "think-outside-the-box", is not bounded by the available nanomaterials, and thus has a high potential of creating next-generation and ground-breaking solutions to the water challenges of our times. In theory, any material developed within the scheme of rational design is new and thus contributes to the already vast library of nanomaterial database. However, it is not highly likely that the nanomaterials designed and produced based on the rational design concept find themselves as effective in the processes other than their designed purposes.

In light of the exciting progress in the field in the past decade, we truly believe that the

rational design of nanomaterials will continue to evolve and offer us with even more unprecedented opportunities to solve the water challenges in a sustainable ways. Looking at the near future, followings are some of our humble expectations: (1) the molecular dynamics and other simulation tools would extend their presence in the field and would gradually be taken in as an indispensable guiding tools in both the problem definition and conceptual design of the nanomaterials steps (Figure 16b); (2) the next few years would see more multi-functional and all-in-one nanomaterials designs for groundbreaking water applications; (3) smart and intelligent nanomaterials, nano-devices, and nano-systems, which are capable of autonomously adjust their function(s) in response to ambient conditions for the purpose of best performing toward their designed goals, would most likely emerge in the water treatment field and be gaining popularity thereafter.

### Acknowledgements:

The authors are grateful to KAUST for very generous funding support. We would like to thank Professor Chuyang Tang from The University of Hong Kong and Dr. Zhenyu Li from the WDRC at KAUST for their suggestions and comments on the membrane section of the review.

### References

1. R. P. Schwarzenbach, T. Egli, T. B. Hofstetter, U. von Gunten and B. Wehrli, *Annual Review of Environment and Resources*, 2010, **35**, 109-136.
2. WHO, *Guidelines for Drinking-water Quality (FOURTH EDITION)*, 2011.
3. M. Rafatullah, O. Sulaiman, R. Hashim and A. Ahmad, *Journal of Hazardous Materials*, 2010, **177**, 70-80.
4. G. Crini, *Bioresource Technology*, 2006, **97**, 1061-1085.
5. S. Babel and T. A. Kurniawan, *Journal of Hazardous Materials*, 2003, **97**, 219-243.
6. V. K. Gupta, I. Ali, T. A. Saleh, A. Nayak and S. Agarwal, *RSC Advances*, 2012, **2**, 6380-6388.
7. B. A. Lyon, R. Y. Milsk, A. B. DeAngelo, J. E. Simmons, M. P. Moyer and H. S. Weinberg, *Environmental Science & Technology*, 2014, **48**, 6743-6753.
8. D. Ghernaout, B. Ghernaout and M. W. Naceur, *Desalination*, 2011, **271**, 1-10.
9. M. Catalá, N. Domínguez-Morueco, A. Migens, R. Molina, F. Martínez, Y. Valcárcel, N. Mastroianni, M. López de Alda, D. Barceló and Y. Segura, *Science of The Total Environment*, 2015, **520**, 198-205.
10. B. Van Der Bruggen, C. Vandecasteele, T. Van Gestel, W. Doyen and R. Leysen, *Environmental Progress*, 2003, **22**, 46-56.
11. M. M. Pendergast and E. M. V. Hoek, *Energy & Environmental Science*, 2011, **4**, 1946-1971.
12. T.-w. Hao, P.-y. Xiang, H. R. Mackey, K. Chi, H. Lu, H.-k. Chui, M. C. M. van Loosdrecht and G.-H. Chen, *Water Research*, 2014, **65**, 1-21.
13. J. P. Scott and D. F. Ollis, *Environmental Progress*, 1995, **14**, 88-103.
14. X.-D. Hao, Q.-L. Wang, J.-Y. Zhu and M. C. M. Van Loosdrecht, *Critical Reviews in Environmental Science and Technology*, 2010, **40**, 239-265.
15. R. P. Feynman, *Microelectromechanical Systems, Journal of*, 1992, **1**, 60-66.

16. M.-C. Daniel and D. Astruc, *Chemical Reviews*, 2004, **104**, 293-346.
17. Y. Xia, P. Yang, Y. Sun, Y. Wu, B. Mayers, B. Gates, Y. Yin, F. Kim and H. Yan, *Advanced Materials*, 2003, **15**, 353-389.
18. R. H. Baughman, A. A. Zakhidov and W. A. de Heer, *Science*, 2002, **297**, 787-792.
19. X. Chen and S. S. Mao, *Chemical Reviews*, 2007, **107**, 2891-2959.
20. E. Ozbay, *Science*, 2006, **311**, 189-193.
21. A. K. Geim and K. S. Novoselov, *Nat Mater*, 2007, **6**, 183-191.
22. C. T. Yavuz, J. T. Mayo, W. W. Yu, A. Prakash, J. C. Falkner, S. Yean, L. Cong, H. J. Shipley, A. Kan, M. Tomson, D. Natelson and V. L. Colvin, *Science*, 2006, **314**, 964-967.
23. Z. Luo, M. Ibáñez, A. M. Antolín, A. Genç, A. Shavel, S. Contreras, F. Medina, J. Arbiol and A. Cabot, *Langmuir*, 2015, **31**, 3952-3957.
24. Y. Wang, D. Chen, Y. Wang, F. Huang, Q. Hu and Z. Lin, *Nanoscale*, 2012, **4**, 3665-3668.
25. L.-F. Chen, H.-W. Liang, Y. Lu, C.-H. Cui and S.-H. Yu, *Langmuir*, 2011, **27**, 8998-9004.
26. Z. Li, D. V. Potapenko and R. M. Osgood, *ACS Nano*, 2015, **9**, 82-87.
27. A. P. Alivisatos, *Science*, 1996, **271**, 933-937.
28. K. Zhou, X. Wang, X. Sun, Q. Peng and Y. Li, *Journal of Catalysis*, 2005, **229**, 206-212.
29. M. L. Mastronardi, K. K. Chen, K. Liao, G. Casillas and G. A. Ozin, *The Journal of Physical Chemistry C*, 2015, **119**, 826-834.
30. A. L. Swindle, A. S. E. Madden, I. M. Cozzarelli and M. Benamara, *Environmental Science & Technology*, 2014, **48**, 11413-11420.
31. S. Liu, J. Yu and M. Jaroniec, *Chemistry of Materials*, 2011, **23**, 4085-4093.
32. S. Liu, J. Yu and M. Jaroniec, *Journal of the American Chemical Society*, 2010, **132**, 11914-11916.
33. Q. Zhang, Y. Zhou, E. Villarreal, Y. Lin, S. Zou and H. Wang, *Nano Letters*, 2015, **15**, 4161-4169.
34. K. L. Kelly, E. Coronado, L. L. Zhao and G. C. Schatz, *The Journal of Physical Chemistry B*, 2003, **107**, 668-677.
35. X. Qu, J. Brame, Q. Li and P. J. J. Alvarez, *Accounts of Chemical Research*, 2013, **46**, 834-843.
36. L. S. Zhong, J. S. Hu, H. P. Liang, A. M. Cao, W. G. Song and L. J. Wan, *Advanced Materials*, 2006, **18**, 2426-2431.
37. W.-x. Zhang, *Journal of Nanoparticle Research*, 2003, **5**, 323-332.
38. M. S. Mauter and M. Elimelech, *Environmental Science & Technology*, 2008, **42**, 5843-5859.
39. P. G. Tratnyek and R. L. Johnson, *Nano Today*, 2006, **1**, 44-48.
40. X. Qu, P. J. J. Alvarez and Q. Li, *Water Research*, 2013, **47**, 3931-3946.
41. X. Quan, S. Yang, X. Ruan and H. Zhao, *Environmental Science & Technology*, 2005, **39**, 3770-3775.
42. S. J. Tesh and T. B. Scott, *Advanced Materials*, 2014, **26**, 6056-6068.
43. J. Li, T. Zhao, T. Chen, Y. Liu, C. N. Ong and J. Xie, *Nanoscale*, 2015, **7**, 7502-7519.
44. M. M. Khin, A. S. Nair, V. J. Babu, R. Murugan and S. Ramakrishna, *Energy & Environmental Science*, 2012, **5**, 8075-8109.
45. Y. Huang and A. A. Keller, *Water Research*, 2015, **80**, 159-168.
46. S. Tao, Y. Wang and Y. An, *Journal of Materials Chemistry*, 2011, **21**, 11901-11907.
47. T. Wang, L. Zhang, C. Li, W. Yang, T. Song, C. Tang, Y. Meng, S. Dai, H. Wang, L. Chai and J. Luo, *Environmental Science & Technology*, 2015, **49**, 5654-5662.
48. Y. Liu, S. Yu, R. Feng, A. Bernard, Y. Liu, Y. Zhang, H. Duan, W. Shang, P. Tao, C. Song and T.

- Deng, *Advanced Materials*, 2015, **27**, 2768-2774.
49. C. Lu, X. Liu, Y. Li, F. Yu, L. Tang, Y. Hu and Y. Ying, *ACS Applied Materials & Interfaces*, 2015, DOI: 10.1021/acsami.5b03423.
50. K. N. Knust, D. Hlushkou, R. K. Anand, U. Tallarek and R. M. Crooks, *Angewandte Chemie International Edition*, 2013, **52**, 8107-8110.
51. Z. Liu, H. Bai and D. D. Sun, *New Journal of Chemistry*, 2011, **35**, 137-140.
52. C. Nützenadel, A. Züttel, D. Chartouni, G. Schmid and L. Schlapbach, *Eur. Phys. J. D*, 2000, **8**, 245-250.
53. J. Gómez-Pastora, E. Bringas and I. Ortiz, *Chemical Engineering Journal*, 2014, **256**, 187-204.
54. J. T. Mayo, C. Yavuz, S. Yean, L. Cong, H. Shipley, W. Yu, J. Falkner, A. Kan, M. Tomson and V. L. Colvin, *Science and Technology of Advanced Materials*, 2007, **8**, 71-75.
55. J. Hu, G. Chen and I. M. C. Lo, *Water Research*, 2005, **39**, 4528-4536.
56. X.-q. Li, D. W. Elliott and W.-x. Zhang, *Critical Reviews in Solid State and Materials Sciences*, 2006, **31**, 111-122.
57. Z.-m. Xiu, Z.-h. Jin, T.-l. Li, S. Mahendra, G. V. Lowry and P. J. J. Alvarez, *Bioresource Technology*, 2010, **101**, 1141-1146.
58. Y. Liu, S. A. Majetich, R. D. Tilton, D. S. Sholl and G. V. Lowry, *Environmental Science & Technology*, 2005, **39**, 1338-1345.
59. J. Gotpagar, E. Grulke, T. Tsang and D. Bhattacharyya, *Environmental Progress*, 1997, **16**, 137-143.
60. A. Taghavy, J. Costanza, K. D. Pennell and L. M. Abriola, *Journal of Contaminant Hydrology*, 2010, **118**, 128-142.
61. J. Zhan, T. Zheng, G. Piringer, C. Day, G. L. McPherson, Y. Lu, K. Papadopoulos and V. T. John, *Environmental Science & Technology*, 2008, **42**, 8871-8876.
62. T. Zheng, J. Zhan, J. He, C. Day, Y. Lu, G. L. McPherson, G. Piringer and V. T. John, *Environmental Science & Technology*, 2008, **42**, 4494-4499.
63. B. Sunkara, J. Zhan, J. He, G. L. McPherson, G. Piringer and V. T. John, *ACS Applied Materials & Interfaces*, 2010, **2**, 2854-2862.
64. Z. Yue and J. Economy, *Journal of Nanoparticle Research*, 2005, **7**, 477-487.
65. Y. Zhang, S. Wei, F. Liu, Y. Du, S. Liu, Y. Ji, T. Yokoi, T. Tatsumi and F.-S. Xiao, *Nano Today*, 2009, **4**, 135-142.
66. S. Singh, V. C. Srivastava and I. D. Mall, *Colloids and Surfaces A: Physicochemical and Engineering Aspects*, 2009, **332**, 50-56.
67. H. Li, Z. Bian, J. Zhu, Y. Huo, H. Li and Y. Lu, *Journal of the American Chemical Society*, 2007, **129**, 4538-4539.
68. J.-J. Li, X.-Y. Xu, Z. Jiang, Z.-P. Hao and C. Hu, *Environmental Science & Technology*, 2005, **39**, 1319-1323.
69. Y. Wang, J. Liu, P. Wang, C. J. Werth and T. J. Strathmann, *ACS Catalysis*, 2014, **4**, 3551-3559.
70. D. Mohan and C. U. Pittman Jr, *Journal of Hazardous Materials*, 2006, **137**, 762-811.
71. A. Bhatnagar, W. Hogland, M. Marques and M. Sillanpää, *Chemical Engineering Journal*, 2013, **219**, 499-511.
72. C. Stoquart, P. Servais, P. R. Bérubé and B. Barbeau, *Journal of Membrane Science*, 2012, **411-412**, 1-12.
73. R. Toor and M. Mohseni, *Chemosphere*, 2007, **66**, 2087-2095.

74. C. Namasivayam and D. Kavitha, *Dyes and Pigments*, 2002, **54**, 47-58.
75. W. Teng, Z. Wu, J. Fan, H. Chen, D. Feng, Y. Lv, J. Wang, A. M. Asiri and D. Zhao, *Energy & Environmental Science*, 2013, **6**, 2765-2776.
76. W.-J. Huang, B.-L. Cheng and Y.-L. Cheng, *Journal of Hazardous Materials*, 2007, **141**, 115-122.
77. G. Whitesides, J. Mathias and C. Seto, *Science*, 1991, **254**, 1312-1319.
78. C. T. Kresge, M. E. Leonowicz, W. J. Roth, J. C. Vartuli and J. S. Beck, *Nature*, 1992, **359**, 710-712.
79. A. Monnier, F. Schüth, Q. Huo, D. Kumar, D. Margolese, R. S. Maxwell, G. D. Stucky, M. Krishnamurty, P. Petroff, A. Firouzi, M. Janicke and B. F. Chmelka, *Science*, 1993, **261**, 1299-1303.
80. Y. Wan and Zhao, *Chemical Reviews*, 2007, **107**, 2821-2860.
81. D. Zhao, J. Feng, Q. Huo, N. Melosh, G. H. Fredrickson, B. F. Chmelka and G. D. Stucky, *Science*, 1998, **279**, 548-552.
82. R. Ryoo, S. H. Joo and S. Jun, *The Journal of Physical Chemistry B*, 1999, **103**, 7743-7746.
83. A. H. Lu and F. Schüth, *Advanced Materials*, 2006, **18**, 1793-1805.
84. Z. Wu, Y. Meng and D. Zhao, *Microporous and Mesoporous Materials*, 2010, **128**, 165-179.
85. C. Liang, K. Hong, G. A. Guiochon, J. W. Mays and S. Dai, *Angewandte Chemie International Edition*, 2004, **43**, 5785-5789.
86. Y. Meng, D. Gu, F. Zhang, Y. Shi, L. Cheng, D. Feng, Z. Wu, Z. Chen, Y. Wan, A. Stein and D. Zhao, *Chemistry of Materials*, 2006, **18**, 4447-4464.
87. Y. Meng, D. Gu, F. Zhang, Y. Shi, H. Yang, Z. Li, C. Yu, B. Tu and D. Zhao, *Angewandte Chemie International Edition*, 2005, **44**, 7053-7059.
88. Y. Wan, Y. Shi and D. Zhao, *Chemistry of Materials*, 2008, **20**, 932-945.
89. F. Zhang, Y. Meng, D. Gu, Yan, C. Yu, B. Tu and D. Zhao, *Journal of the American Chemical Society*, 2005, **127**, 13508-13509.
90. Z. Wu, P. A. Webley and D. Zhao, *Langmuir*, 2010, **26**, 10277-10286.
91. K. Wang, H. Yang, L. Zhu, Z. Ma, S. Xing, Q. Lv, J. Liao, C. Liu and W. Xing, *Electrochimica Acta*, 2009, **54**, 4626-4630.
92. L. C. C. d. Silva, L. B. O. d. Santos, G. Abate, I. C. Cosentino, M. C. A. Fantini, J. C. Masini and J. R. Matos, *Microporous and Mesoporous Materials*, 2008, **110**, 250-259.
93. Z. Wu, Y. Yang, B. Tu, P. Webley and D. Zhao, *Adsorption*, 2009, **15**, 123-132.
94. E. M. Jochimsen, W. W. Carmichael, J. An, D. M. Cardo, S. T. Cookson, C. E. M. Holmes, M. B. Antunes, D. A. de Melo Filho, T. M. Lyra, V. S. T. Barreto, S. M. F. O. Azevedo and W. R. Jarvis, *New England Journal of Medicine*, 1998, **338**, 873-878.
95. P. Pendleton, R. Schumann and S. H. Wong, *Journal of Colloid and Interface Science*, 2001, **240**, 1-8.
96. Y. Deng, D. Qi, C. Deng, X. Zhang and D. Zhao, *Journal of the American Chemical Society*, 2008, **130**, 28-29.
97. W. Teng, Z. Wu, D. Feng, J. Fan, J. Wang, H. Wei, M. Song and D. Zhao, *Environmental Science & Technology*, 2013, **47**, 8633-8641.
98. M. Naguib, V. N. Mochalin, M. W. Barsoum and Y. Gogotsi, *Advanced Materials*, 2014, **26**, 992-1005.
99. Q. Liu, J. Shi, J. Sun, T. Wang, L. Zeng and G. Jiang, *Angewandte Chemie International Edition*, 2011, **50**, 5913-5917.

100. B. Mi, *Science*, 2014, **343**, 740-742.
101. R. K. Joshi, P. Carbone, F. C. Wang, V. G. Kravets, Y. Su, I. V. Grigorieva, H. A. Wu, A. K. Geim and R. R. Nair, *Science*, 2014, **343**, 752-754.
102. X. Dong, J. Chen, Y. Ma, J. Wang, M. B. Chan-Park, X. Liu, L. Wang, W. Huang and P. Chen, *Chemical Communications*, 2012, **48**, 10660-10662.
103. D. N. H. Tran, S. Kabiri, T. R. Sim and D. Losic, *Environmental Science: Water Research & Technology*, 2015, **1**, 298-305.
104. H. Bi, X. Xie, K. Yin, Y. Zhou, S. Wan, L. He, F. Xu, F. Banhart, L. Sun and R. S. Ruoff, *Advanced Functional Materials*, 2012, **22**, 4421-4425.
105. M. Naguib, M. Kurtoglu, V. Presser, J. Lu, J. Niu, M. Heon, L. Hultman, Y. Gogotsi and M. W. Barsoum, *Advanced Materials*, 2011, **23**, 4248-4253.
106. M. R. Lukatskaya, O. Mashtalir, C. E. Ren, Y. Dall'Agnese, P. Rozier, P. L. Taberna, M. Naguib, P. Simon, M. W. Barsoum and Y. Gogotsi, *Science*, 2013, **341**, 1502-1505.
107. L. Mercier and T. J. Pinnavaia, *Advanced Materials*, 1997, **9**, 500-503.
108. A. Walcarius and L. Mercier, *Journal of Materials Chemistry*, 2010, **20**, 4478-4511.
109. L. Mercier and T. J. Pinnavaia, *Environmental Science & Technology*, 1998, **32**, 2749-2754.
110. X. Luo, F. Deng, L. Min, S. Luo, B. Guo, G. Zeng and C. Au, *Environmental Science & Technology*, 2013, **47**, 7404-7412.
111. R. D. Hancock and A. E. Martell, *Chemical Reviews*, 1989, **89**, 1875-1914.
112. A. Bibby and L. Mercier, *Chemistry of Materials*, 2002, **14**, 1591-1597.
113. G. Li, Z. Zhao, J. Liu and G. Jiang, *Journal of Hazardous Materials*, 2011, **192**, 277-283.
114. F. Hoffmann, M. Cornelius, J. Morell and M. Fröba, *Angewandte Chemie International Edition*, 2006, **45**, 3216-3251.
115. P. K. Jal, S. Patel and B. K. Mishra, *Talanta*, 2004, **62**, 1005-1028.
116. A. Stein, B. J. Melde and R. C. Schroden, *Advanced Materials*, 2000, **12**, 1403-1419.
117. X. Feng, G. E. Fryxell, L.-Q. Wang, A. Y. Kim, J. Liu and K. M. Kemner, *Science*, 1997, **276**, 923-926.
118. J. Aguado, J. M. Arsuaga and A. Arencibia, *Microporous and Mesoporous Materials*, 2008, **109**, 513-524.
119. A. M. Liu, K. Hidajat, S. Kawi and D. Y. Zhao, *Chemical Communications*, 2000, DOI: 10.1039/b002661i, 1145-1146.
120. A. Heidari, H. Younesi and Z. Mehraban, *Chemical Engineering Journal*, 2009, **153**, 70-79.
121. A. Shahbazi, H. Younesi and A. Badiiei, *Chemical Engineering Journal*, 2011, **168**, 505-518.
122. C. Wang, S. Tao, W. Wei, C. Meng, F. Liu and M. Han, *Journal of Materials Chemistry*, 2010, **20**, 4635-4641.
123. B. Li, Y. Zhang, D. Ma, Z. Shi and S. Ma, *Nat Commun*, 2014, **5**.
124. I. G. B. Kaya, D. Duranoglu, U. Beker and B. F. Senkal, *CLEAN – Soil, Air, Water*, 2011, **39**, 980-988.
125. B. Pan, B. Pan, W. Zhang, L. Lv, Q. Zhang and S. Zheng, *Chemical Engineering Journal*, 2009, **151**, 19-29.
126. S. P. Mishra, S. S. Dubey and D. Tiwari, *Journal of Colloid and Interface Science*, 2004, **279**, 61-67.
127. A. Afkhami, M. Saber-Tehrani and H. Bagheri, *Journal of Hazardous Materials*, 2010, **181**, 836-844.

128. M. Hua, S. Zhang, B. Pan, W. Zhang, L. Lv and Q. Zhang, *Journal of Hazardous Materials*, 2012, **211–212**, 317-331.
129. X. Mi, G. Huang, W. Xie, W. Wang, Y. Liu and J. Gao, *Carbon*, 2012, **50**, 4856-4864.
130. G. K. Ramesha, A. Vijaya Kumara, H. B. Muralidhara and S. Sampath, *Journal of Colloid and Interface Science*, 2011, **361**, 270-277.
131. Q. Peng, J. Guo, Q. Zhang, J. Xiang, B. Liu, A. Zhou, R. Liu and Y. Tian, *Journal of the American Chemical Society*, 2014, **136**, 4113-4116.
132. Y. Ying, Y. Liu, X. Wang, Y. Mao, W. Cao, P. Hu and X. Peng, *ACS Applied Materials & Interfaces*, 2015, **7**, 1795-1803.
133. O. Mashtalir, K. M. Cook, V. N. Mochalin, M. Crowe, M. W. Barsoum and Y. Gogotsi, *Journal of Materials Chemistry A*, 2014, **2**, 14334-14338.
134. D. Mohan and C. U. Pittman Jr, *Journal of Hazardous Materials*, 2007, **142**, 1-53.
135. S. Chakravarty, V. Dureja, G. Bhattacharyya, S. Maity and S. Bhattacharjee, *Water Research*, 2002, **36**, 625-632.
136. B. Daus, R. Wennrich and H. Weiss, *Water Research*, 2004, **38**, 2948-2954.
137. H. Liu, K. Zuo and C. D. Vecitis, *Environmental Science & Technology*, 2014, **48**, 13871-13879.
138. M. Dakiky, M. Khamis, A. Manassra and M. Mer'eb, *Advances in Environmental Research*, 2002, **6**, 533-540.
139. A. Ramana; and A. K. Sengupta, *Journal of Environmental Engineering*, 1992, **118**, 755-775.
140. G. E. Fryxell, J. Liu, T. A. Hauser, Z. Nie, K. F. Ferris, S. Mattigod, M. Gong and R. T. Hallen, *Chemistry of Materials*, 1999, **11**, 2148-2154.
141. H. Yoshitake, T. Yokoi and T. Tatsumi, *Chemistry of Materials*, 2003, **15**, 1713-1721.
142. T. Yokoi, T. Tatsumi and H. Yoshitake, *Journal of Colloid and Interface Science*, 2004, **274**, 451-457.
143. J. A. Lackovic, N. P. Nikolaidis and G. M. Dobbs, *Environmental Engineering Science*, 2000, **17**, 29-39.
144. Y.-F. Lin and J.-L. Chen, *RSC Advances*, 2013, **3**, 15344-15349.
145. P. Wang and I. M. C. Lo, *Water Research*, 2009, **43**, 3727-3734.
146. B. Chen, Z. Zhu, J. Hong, Z. Wen, J. Ma, Y. Qiu and J. Chen, *Dalton Transactions*, 2014, **43**, 10767-10777.
147. Z. Wu, W. Li, P. A. Webley and D. Zhao, *Advanced Materials*, 2012, **24**, 485-491.
148. J. Yang, H. Zhang, M. Yu, I. Emmanuelawati, J. Zou, Z. Yuan and C. Yu, *Advanced Functional Materials*, 2014, **24**, 1354-1363.
149. G. Lee, C. Chen, S.-T. Yang and W.-S. Ahn, *Microporous and Mesoporous Materials*, 2010, **127**, 152-156.
150. J. He and J. P. Chen, *Journal of Colloid and Interface Science*, 2014, **416**, 227-234.
151. Q. Zhang, Q. Du, T. Jiao, Z. Zhang, S. Wang, Q. Sun and F. Gao, *Scientific Reports*, 2013, **3**, 2551.
152. J. M. Blais, D. W. Schindler, D. C. G. Muir, L. E. Kimpe, D. B. Donald and B. Rosenberg, *Nature*, 1998, **395**, 585-588.
153. M. T. O. Jonker, S. A. van der Heijden, J. P. Kreitinger and S. B. Hawthorne, *Environmental Science & Technology*, 2007, **41**, 7472-7478.
154. A. G. Carr, R. Mammucari and N. R. Foster, *Chemical Engineering Journal*, 2011, **172**, 1-17.
155. P. Wang and A. A. Keller, *Water Research*, 2008, **42**, 2093-2101.

156. P. Wang and A. A. Keller, *Water Research*, 2009, **43**, 706-714.
157. C. T. Jafvert, *Environmental Science & Technology*, 1991, **25**, 1039-1045.
158. R. Denoyel and E. Sabio Rey, *Langmuir*, 1998, **14**, 7321-7323.
159. K. Hanna, I. Beurroies, R. Denoyel, D. Desplandier-Giscard, A. Galarneau and F. Di Renzo, *Journal of Colloid and Interface Science*, 2002, **252**, 276-283.
160. P. Wang, Q. Shi, Y. Shi, K. K. Clark, G. D. Stucky and A. A. Keller, *Journal of the American Chemical Society*, 2009, **131**, 182-188.
161. Y. Shi, B. Li, P. Wang, R. Dua and D. Zhao, *Microporous and Mesoporous Materials*, 2012, **155**, 252-257.
162. X.-l. Zhang, H.-y. Niu, W.-h. Li, Y.-l. Shi and Y.-q. Cai, *Chemical Communications*, 2011, **47**, 4454-4456.
163. B. Pan, P. Ning and B. Xing, *Environmental Science and Pollution Research*, 2009, **16**, 106-116.
164. J. Xu, L. Wu and A. C. Chang, *Chemosphere*, 2009, **77**, 1299-1305.
165. S. Suárez, M. Carballa, F. Omil and J. Lema, *Rev Environ Sci Biotechnol*, 2008, **7**, 125-138.
166. X. Shen, L. Zhu, N. Wang, L. Ye and H. Tang, *Chemical Communications*, 2012, **48**, 788-798.
167. L. Chen, S. Xu and J. Li, *Chemical Society Reviews*, 2011, **40**, 2922-2942.
168. T. Takeuchi and J. Haginaka, *Journal of Chromatography B: Biomedical Sciences and Applications*, 1999, **728**, 1-20.
169. S. Tombelli, M. Minunni and M. Mascini, *Biosensors and Bioelectronics*, 2005, **20**, 2424-2434.
170. S. Tombelli, M. Minunni and M. Mascini, *Biomolecular Engineering*, 2007, **24**, 191-200.
171. C. Tuerk and L. Gold, *Science*, 1990, **249**, 505-510.
172. A. D. Ellington and J. W. Szostak, *Nature*, 1990, **346**, 818-822.
173. M. Kim, H.-J. Um, S. Bang, S.-H. Lee, S.-J. Oh, J.-H. Han, K.-W. Kim, J. Min and Y.-H. Kim, *Environmental Science & Technology*, 2009, **43**, 9335-9340.
174. X. Hu, L. Mu, Q. Zhou, J. Wen and J. Pawliszyn, *Environmental Science & Technology*, 2011, **45**, 4890-4895.
175. Y. Li, X. Li, J. Chu, C. Dong, J. Qi and Y. Yuan, *Environmental Pollution*, 2010, **158**, 2317-2323.
176. Y. Li, C. Dong, J. Chu, J. Qi and X. Li, *Nanoscale*, 2011, **3**, 280-287.
177. B. Liu, M. Han, G. Guan, S. Wang, R. Liu and Z. Zhang, *The Journal of Physical Chemistry C*, 2011, **115**, 17320-17327.
178. M.-H. Lee, J. L. Thomas, M.-H. Ho, C. Yuan and H.-Y. Lin, *ACS Applied Materials & Interfaces*, 2010, **2**, 1729-1736.
179. L. Chang, S. Chen and X. Li, *Applied Surface Science*, 2012, **258**, 6660-6664.
180. S. Xu, C. Guo, Y. Li, Z. Yu, C. Wei and Y. Tang, *Journal of Hazardous Materials*, 2014, **264**, 34-41.
181. X. Shen, L. Zhu, J. Li and H. Tang, *Chemical Communications*, 2007, DOI: 10.1039/b615303h, 1163-1165.
182. X. Shen, L. Zhu, G. Liu, H. Yu and H. Tang, *Environmental Science & Technology*, 2008, **42**, 1687-1692.
183. X. Shen, L. Zhu, H. Yu, H. Tang, S. Liu and W. Li, *New Journal of Chemistry*, 2009, **33**, 1673-1679.
184. J. J. Pignatello, E. Oliveros and A. MacKay, *Critical Reviews in Environmental Science and Technology*, 2006, **36**, 1-84.
185. E. Erdim, A. R. Badireddy and M. R. Wiesner, *Journal of Hazardous Materials*, 2015, **283**,

- 80-88.
186. E. Neyens and J. Baeyens, *Journal of Hazardous Materials*, 2003, **98**, 33-50.
187. M. C. Pereira, L. C. A. Oliveira and E. Murad, *Clay Minerals*, 2012, **47**, 285-302.
188. K. Rusevova, F.-D. Kopinke and A. Georgi, *Journal of Hazardous Materials*, 2012, **241-242**, 433-440.
189. W. G. Kuo, *Water Research*, 1992, **26**, 881-886.
190. E. Lipczynska-Kochany, G. Sprah and S. Harms, *Chemosphere*, 1995, **30**, 9-20.
191. H. Gallard, J. De Laat and B. Legube, *Water Research*, 1999, **33**, 2929-2936.
192. C. F. Wells and M. A. Salam, *Journal of the Chemical Society A: Inorganic, Physical, Theoretical*, 1968, DOI: 10.1039/j19680000024, 24-29.
193. K. Fajferberg and H. Debellefontaine, *Applied Catalysis B: Environmental*, 1996, **10**, L229-L235.
194. W. Z. Tang and R. Z. Chen, *Chemosphere*, 1996, **32**, 947-958.
195. F. Lücking, H. Köser, M. Jank and A. Ritter, *Water Research*, 1998, **32**, 2607-2614.
196. E. G. Garrido-Ramírez, B. K. G. Theng and M. L. Mora, *Applied Clay Science*, 2010, **47**, 182-192.
197. A. Dhakshinamoorthy, S. Navalon, M. Alvaro and H. Garcia, *ChemSusChem*, 2012, **5**, 46-64.
198. M. A. Voinov, J. O. S. Pagán, E. Morrison, T. I. Smirnova and A. I. Smirnov, *Journal of the American Chemical Society*, 2011, **133**, 35-41.
199. I. R. Guimarães, L. C. A. Oliveira, P. F. Queiroz, T. C. Ramalho, M. Pereira, J. D. Fabris and J. D. Ardisson, *Applied Catalysis A: General*, 2008, **347**, 89-93.
200. S. Rahim Pouran, A. A. Abdul Raman and W. M. A. Wan Daud, *Journal of Cleaner Production*, 2014, **64**, 24-35.
201. R. G. Zepp, B. C. Faust and J. Hoigne, *Environmental Science & Technology*, 1992, **26**, 313-319.
202. R. F. P. Nogueira, M. C. Oliveira and W. C. Paterlini, *Talanta*, 2005, **66**, 86-91.
203. P. L. Huston and J. J. Pignatello, *Water Research*, 1999, **33**, 1238-1246.
204. Z. Miao, S. Tao, Y. Wang, Y. Yu, C. Meng and Y. An, *Microporous and Mesoporous Materials*, 2013, **176**, 178-185.
205. S. Esplugas, J. Giménez, S. Contreras, E. Pascual and M. Rodríguez, *Water Research*, 2002, **36**, 1034-1042.
206. E. Brillas, I. Sirés and M. A. Oturan, *Chemical Reviews*, 2009, **109**, 6570-6631.
207. S. Khoufi, F. Aloui and S. Sayadi, *Water Research*, 2006, **40**, 2007-2016.
208. H. Liu, C. Wang, Xiangzhong, X. Xuan, C. Jiang and H. n. Cui, *Environmental Science & Technology*, 2007, **41**, 2937-2942.
209. J. H. Ramirez, F. J. Maldonado-Hódar, A. F. Pérez-Cadenas, C. Moreno-Castilla, C. A. Costa and L. M. Madeira, *Applied Catalysis B: Environmental*, 2007, **75**, 312-323.
210. K. Dutta, S. Mukhopadhyay, S. Bhattacharjee and B. Chaudhuri, *Journal of Hazardous Materials*, 2001, **84**, 57-71.
211. R. Andreozzi, V. Caprio, A. Insola and R. Marotta, *Catalysis Today*, 1999, **53**, 51-59.
212. M. M. Huber, S. Canonica, G.-Y. Park and U. von Gunten, *Environmental Science & Technology*, 2003, **37**, 1016-1024.
213. M. R. Hoffmann, S. T. Martin, W. Choi and D. W. Bahnemann, *Chemical Reviews*, 1995, **95**, 69-96.
214. X. Chen and C. Burda, *Journal of the American Chemical Society*, 2008, **130**, 5018-5019.
215. Z. Zhang and P. Wang, *Energy & Environmental Science*, 2012, **5**, 6506-6512.

216. R. Asahi, T. Morikawa, T. Ohwaki, K. Aoki and Y. Taga, *Science*, 2001, **293**, 269-271.
217. F. Zuo, L. Wang, T. Wu, Z. Zhang, D. Borchardt and P. Feng, *Journal of the American Chemical Society*, 2010, **132**, 11856-11857.
218. T. L. Thompson and J. T. Yates, *Chemical Reviews*, 2006, **106**, 4428-4453.
219. I. Justicia, P. Ordejón, G. Canto, J. L. Mozos, J. Fraxedas, G. A. Battiston, R. Gerbasi and A. Figueras, *Advanced Materials*, 2002, **14**, 1399-1402.
220. Z. Zhang, M. N. Hedhili, H. Zhu and P. Wang, *Physical Chemistry Chemical Physics*, 2013, **15**, 15637-15644.
221. Z. Zhang, X. Yang, M. N. Hedhili, E. Ahmed, L. Shi and P. Wang, *ACS Applied Materials & Interfaces*, 2014, **6**, 691-696.
222. X. Chen, L. Liu, P. Y. Yu and S. S. Mao, *Science*, 2011, **331**, 746-750.
223. X. Chen, L. Liu and F. Huang, *Chemical Society Reviews*, 2015, **44**, 1861-1885.
224. N. Liu, C. Schneider, D. Freitag, M. Hartmann, U. Venkatesan, J. Müller, E. Spiecker and P. Schmuki, *Nano Letters*, 2014, **14**, 3309-3313.
225. H. Yin, T. Lin, C. Yang, Z. Wang, G. Zhu, T. Xu, X. Xie, F. Huang and M. Jiang, *Chemistry – A European Journal*, 2013, **19**, 13313-13316.
226. Y. Tian and T. Tatsuma, *Journal of the American Chemical Society*, 2005, **127**, 7632-7637.
227. Z. Zhang, L. Zhang, M. N. Hedhili, H. Zhang and P. Wang, *Nano Letters*, 2013, **13**, 14-20.
228. M. Pelaez, N. T. Nolan, S. C. Pillai, M. K. Seery, P. Falaras, A. G. Kontos, P. S. M. Dunlop, J. W. J. Hamilton, J. A. Byrne, K. O'Shea, M. H. Entezari and D. D. Dionysiou, *Applied Catalysis B: Environmental*, 2012, **125**, 331-349.
229. Z. Zhang, Y. Yu and P. Wang, *ACS Applied Materials & Interfaces*, 2012, **4**, 990-996.
230. M. Liu, N. de Leon Snapp and H. Park, *Chemical Science*, 2011, **2**, 80-87.
231. H. Tang, K. Prasad, R. Sanjinès, P. E. Schmid and F. Lévy, *Journal of Applied Physics*, 1994, **75**, 2042-2047.
232. M. Takahashi, K. Tsukigi, T. Uchino and T. Yoko, *Thin Solid Films*, 2001, **388**, 231-236.
233. L. C. Kao, C. J. Lin, C. L. Dong, C. L. Chen and S. Y. H. Liou, *Chemical Communications*, 2015, **51**, 6361-6364.
234. X. Zhang, J. H. Pan, A. J. Du, W. Fu, D. D. Sun and J. O. Leckie, *Water Research*, 2009, **43**, 1179-1186.
235. Z. Bian, J. Zhu, F. Cao, Y. Huo, Y. Lu and H. Li, *Chemical Communications*, 2010, **46**, 8451-8453.
236. P. Si, S. Ding, J. Yuan, X. W. Lou and D.-H. Kim, *ACS Nano*, 2011, **5**, 7617-7626.
237. Z. Zhang, Yuan, G. Shi, Y. Fang, L. Liang, H. Ding and L. Jin, *Environmental Science & Technology*, 2007, **41**, 6259-6263.
238. J. M. Macák, H. Tsuchiya and P. Schmuki, *Angewandte Chemie International Edition*, 2005, **44**, 2100-2102.
239. M. M. Abu-Omar and J. H. Espenson, *Inorganic Chemistry*, 1995, **34**, 6239-6240.
240. X.-Q. Gong and A. Selloni, *The Journal of Physical Chemistry B*, 2005, **109**, 19560-19562.
241. D. Zhang, G. Li, X. Yang and J. C. Yu, *Chemical Communications*, 2009, DOI: 10.1039/b907963g, 4381-4383.
242. H. G. Yang, C. H. Sun, S. Z. Qiao, J. Zou, G. Liu, S. C. Smith, H. M. Cheng and G. Q. Lu, *Nature*, 2008, **453**, 638-641.
243. J. A. Byrne, B. R. Eggins, N. M. D. Brown, B. McKinney and M. Rouse, *Applied Catalysis B: Environmental*, 1998, **17**, 25-36.

244. S. Malato, J. Blanco, J. Cáceres, A. R. Fernández-Alba, A. Agüera and A. Rodríguez, *Catalysis Today*, 2002, **76**, 209-220.
245. S.-Y. Lee and S.-J. Park, *Journal of Industrial and Engineering Chemistry*, 2013, **19**, 1761-1769.
246. X. Z. Li, H. L. Liu, P. T. Yue and Y. P. Sun, *Environmental Science & Technology*, 2000, **34**, 4401-4406.
247. D. H. Kim and M. A. Anderson, *Environmental Science & Technology*, 1994, **28**, 479-483.
248. X. Z. Li and H. S. Liu, *Environmental Science & Technology*, 2005, **39**, 4614-4620.
249. R. Abe, *Journal of Photochemistry and Photobiology C: Photochemistry Reviews*, 2010, **11**, 179-209.
250. A. Kudo and Y. Miseki, *Chemical Society Reviews*, 2009, **38**, 253-278.
251. Z. Liu, X. Zhang, S. Nishimoto, M. Jin, D. A. Tryk, T. Murakami and A. Fujishima, *The Journal of Physical Chemistry C*, 2008, **112**, 253-259.
252. A. Fujishima and K. Honda, *Nature*, 1972, **238**, 37-38.
253. J. Gong, Y. Lai and C. Lin, *Electrochimica Acta*, 2010, **55**, 4776-4782.
254. S. U. M. Khan, M. Al-Shahry and W. B. Ingler, *Science*, 2002, **297**, 2243-2245.
255. B.-Z. Wu, H.-Y. Chen, S. J. Wang, C. M. Wai, W. Liao and K. Chiu, *Chemosphere*, 2012, **88**, 757-768.
256. W. S. Orth and R. W. Gillham, *Environmental Science & Technology*, 1996, **30**, 66-71.
257. C.-B. Wang and W.-x. Zhang, *Environmental Science & Technology*, 1997, **31**, 2154-2156.
258. J. Liu, J. K. Choe, Y. Wang, J. R. Shapley, C. J. Werth and T. J. Strathmann, *ACS Catalysis*, 2015, **5**, 511-522.
259. M. M. Abu-Omar, E. H. Appelman and J. H. Espenson, *Inorganic Chemistry*, 1996, **35**, 7751-7757.
260. M. M. Abu-Omar, L. D. McPherson, J. Arias and V. M. Béreau, *Angewandte Chemie International Edition*, 2000, **39**, 4310-4313.
261. K. D. Hurley and J. R. Shapley, *Environmental Science & Technology*, 2007, **41**, 2044-2049.
262. K. D. Hurley, Y. Zhang and J. R. Shapley, *Journal of the American Chemical Society*, 2009, **131**, 14172-14173.
263. J. K. Choe, J. R. Shapley, T. J. Strathmann and C. J. Werth, *Environmental Science & Technology*, 2010, **44**, 4716-4721.
264. Y.-N. Kim, Y.-C. Lee and M. Choi, *Carbon*, 2013, **65**, 315-323.
265. J. K. Choe, M. H. Mehnert, J. S. Guest, T. J. Strathmann and C. J. Werth, *Environmental Science & Technology*, 2013, **47**, 4644-4652.
266. M. G. Davie, K. Shih, F. A. Pacheco, J. O. Leckie and M. Reinhard, *Environmental Science & Technology*, 2008, **42**, 3040-3046.
267. D. Shuai, D. C. McCalman, J. K. Choe, J. R. Shapley, W. F. Schneider and C. J. Werth, *ACS Catalysis*, 2013, **3**, 453-463.
268. J. Yin and B. Deng, *Journal of Membrane Science*, 2015, **479**, 256-275.
269. A. Subramani and J. G. Jacangelo, *Water Research*, 2015, **75**, 164-187.
270. D. Li and H. Wang, *Journal of Materials Chemistry*, 2010, **20**, 4551-4566.
271. K. P. Lee, T. C. Arnot and D. Mattia, *Journal of Membrane Science*, 2011, **370**, 1-22.
272. C. Tang, Z. Wang, I. Petrinić, A. G. Fane and C. Hélix-Nielsen, *Desalination*, 2015, **368**, 89-105.
273. H. M. Hegab and L. Zou, *Journal of Membrane Science*, 2015, **484**, 95-106.
274. N. Ma, J. Wei, S. Qi, Y. Zhao, Y. Gao and C. Y. Tang, *Journal of Membrane Science*, 2013, **441**,

- 54-62.
275. L.-x. Dong, H.-w. Yang, S.-t. Liu, X.-m. Wang and Y. F. Xie, *Desalination*, 2015, **365**, 70-78.
276. K. Lutcmiah, A. R. D. Verliefde, K. Roest, L. C. Rietveld and E. R. Cornelissen, *Water Research*, 2014, **58**, 179-197.
277. C. A. Crock, A. R. Rogensues, W. Shan and V. V. Tarabara, *Water Research*, 2013, **47**, 3984-3996.
278. P. P. Mane, P.-K. Park, H. Hyung, J. C. Brown and J.-H. Kim, *Journal of Membrane Science*, 2009, **338**, 119-127.
279. W. J. Lau, A. F. Ismail, N. Misdan and M. A. Kassim, *Desalination*, 2012, **287**, 190-199.
280. J. Wei, C. Qiu, C. Y. Tang, R. Wang and A. G. Fane, *Journal of Membrane Science*, 2011, **372**, 292-302.
281. N. Y. Yip, A. Tiraferri, W. A. Phillip, J. D. Schiffman and M. Elimelech, *Environmental Science & Technology*, 2010, **44**, 3812-3818.
282. J. E. Cadotte, R. J. Petersen, R. E. Larson and E. E. Erickson, *Desalination*, 1980, **32**, 25-31.
283. M. L. Lind, A. K. Ghosh, A. Jawor, X. Huang, W. Hou, Y. Yang and E. M. V. Hoek, *Langmuir*, 2009, **25**, 10139-10145.
284. H. S. Lee, S. J. Im, J. H. Kim, H. J. Kim, J. P. Kim and B. R. Min, *Desalination*, 2008, **219**, 48-56.
285. M. L. Lind, B.-H. Jeong, A. Subramani, X. Huang and E. M. V. Hoek, *Journal of Materials Research*, 2009, **24**, 1624-1631.
286. B.-H. Jeong, E. M. V. Hoek, Y. Yan, A. Subramani, X. Huang, G. Hurwitz, A. K. Ghosh and A. Jawor, *Journal of Membrane Science*, 2007, **294**, 1-7.
287. M. Kazemimoghadam, *Desalination*, 2010, **251**, 176-180.
288. G. Hummer, J. C. Rasaiah and J. P. Noworyta, *Nature*, 2001, **414**, 188-190.
289. A. Kalra, S. Garde and G. Hummer, *Proceedings of the National Academy of Sciences*, 2003, **100**, 10175-10180.
290. L. Zhang, G.-Z. Shi, S. Qiu, L.-H. Cheng and H.-L. Chen, *Desalination and Water Treatment*, 2011, **34**, 19-24.
291. G. L. Jadao and P. S. Singh, *Journal of Membrane Science*, 2009, **328**, 257-267.
292. J. Yin, E.-S. Kim, J. Yang and B. Deng, *Journal of Membrane Science*, 2012, **423-424**, 238-246.
293. P. Agre, M. Bonhivers and M. J. Borgia, *Journal of Biological Chemistry*, 1998, **273**, 14659-14662.
294. M. Kumar, M. Grzelakowski, J. Zilles, M. Clark and W. Meier, *Proceedings of the National Academy of Sciences*, 2007, **104**, 20719-20724.
295. Y. Zhao, C. Qiu, X. Li, A. Vararattanavech, W. Shen, J. Torres, C. Hélix-Nielsen, R. Wang, X. Hu, A. G. Fane and C. Y. Tang, *Journal of Membrane Science*, 2012, **423-424**, 422-428.
296. J. R. McCutcheon and M. Elimelech, *Journal of Membrane Science*, 2006, **284**, 237-247.
297. S. S. Sablani, M. F. A. Goosen, R. Al-Belushi and M. Wilf, *Desalination*, 2001, **141**, 269-289.
298. E. Matthiasson and B. Sivik, *Desalination*, 1980, **35**, 59-103.
299. G. T. Gray, J. R. McCutcheon and M. Elimelech, *Desalination*, 2006, **197**, 1-8.
300. S. Zhang, K. Y. Wang, T.-S. Chung, H. Chen, Y. C. Jean and G. Amy, *Journal of Membrane Science*, 2010, **360**, 522-535.
301. T. Y. Cath, A. E. Childress and M. Elimelech, *Journal of Membrane Science*, 2006, **281**, 70-87.
302. X. Song, Z. Liu and D. D. Sun, *Advanced Materials*, 2011, **23**, 3256-3260.
303. J. R. McCutcheon and M. Elimelech, *AIChE Journal*, 2007, **53**, 1736-1744.

304. X. Lu, L. H. Arias Chavez, S. Romero-Vargas Castrillón, J. Ma and M. Elimelech, *Environmental Science & Technology*, 2015, **49**, 1436-1444.
305. K. R. Zodrow, E. Bar-Zeev, M. J. Giannetto and M. Elimelech, *Environmental Science & Technology*, 2014, **48**, 13155-13164.
306. M. Ben-Sasson, X. Lu, E. Bar-Zeev, K. R. Zodrow, S. Nejati, G. Qi, E. P. Giannelis and M. Elimelech, *Water Research*, 2014, **62**, 260-270.
307. D. Rana, Y. Kim, T. Matsuura and H. A. Arafat, *Journal of Membrane Science*, 2011, **367**, 110-118.
308. E. M. Vrijenhoek, S. Hong and M. Elimelech, *Journal of Membrane Science*, 2001, **188**, 115-128.
309. D. L. Shaffer, H. Jaramillo, S. Romero-Vargas Castrillón, X. Lu and M. Elimelech, *Journal of Membrane Science*, 2015, **490**, 209-219.
310. D. Rana and T. Matsuura, *Chemical Reviews*, 2010, **110**, 2448-2471.
311. X. Lu, S. Romero-Vargas Castrillón, D. L. Shaffer, J. Ma and M. Elimelech, *Environmental Science & Technology*, 2013, **47**, 12219-12228.
312. T.-H. Bae, I.-C. Kim and T.-M. Tak, *Journal of Membrane Science*, 2006, **275**, 1-5.
313. G.-d. Kang and Y.-m. Cao, *Water Research*, 2012, **46**, 584-600.
314. A. Nabe, E. Staude and G. Belfort, *Journal of Membrane Science*, 1997, **133**, 57-72.
315. G. Kang, M. Liu, B. Lin, Y. Cao and Q. Yuan, *Polymer*, 2007, **48**, 1165-1170.
316. M. Kobayashi, Y. Terayama, H. Yamaguchi, M. Terada, D. Murakami, K. Ishihara and A. Takahara, *Langmuir*, 2012, **28**, 7212-7222.
317. H.-L. Yang, J. C.-T. Lin and C. Huang, *Water Research*, 2009, **43**, 3777-3786.
318. M. S. Rahaman, H. Therien-Aubin, M. Ben-Sasson, C. K. Ober, M. Nielsen and M. Elimelech, *Journal of Materials Chemistry B*, 2014, **2**, 1724-1732.
319. S. Kang, M. Pinault, L. D. Pfefferle and M. Elimelech, *Langmuir*, 2007, **23**, 8670-8673.
320. S. Aslan, M. Deneufchatel, S. Hashmi, N. Li, L. D. Pfefferle, M. Elimelech, E. Pauthe and P. R. Van Tassel, *Journal of Colloid and Interface Science*, 2012, **388**, 268-273.
321. S. Aslan, J. Maatta, B. Z. Haznedaroglu, J. P. M. Goodman, L. D. Pfefferle, M. Elimelech, E. Pauthe, M. Sammalkorpi and P. R. Van Tassel, *Soft Matter*, 2013, **9**, 2136-2144.
322. J. Chen, H. Peng, X. Wang, F. Shao, Z. Yuan and H. Han, *Nanoscale*, 2014, **6**, 1879-1889.
323. F. Perreault, A. F. de Faria, S. Nejati and M. Elimelech, *ACS Nano*, 2015, DOI: 10.1021/acsnano.5b02067.
324. F. Perreault, M. E. Tousley and M. Elimelech, *Environmental Science & Technology Letters*, 2014, **1**, 71-76.
325. D. Konatham, J. Yu, T. A. Ho and A. Striolo, *Langmuir*, 2013, **29**, 11884-11897.
326. D. Cohen-Tanugi and J. C. Grossman, *Nano Letters*, 2012, **12**, 3602-3608.
327. M. E. Suk and N. R. Aluru, *The Journal of Physical Chemistry Letters*, 2010, **1**, 1590-1594.
328. K. Zhao and H. Wu, *Nano Letters*, 2015, **15**, 3664-3668.
329. H. Y. Yang, Z. J. Han, S. F. Yu, K. L. Pey, K. Ostrikov and R. Karnik, *Nat Commun*, 2013, **4**.
330. S. P. Surwade, S. N. Smirnov, I. V. Vlasiouk, R. R. Unocic, G. M. Veith, S. Dai and S. M. Mahurin, *Nat Nano*, 2015, **10**, 459-464.
331. R. R. Nair, H. A. Wu, P. N. Jayaram, I. V. Grigorieva and A. K. Geim, *Science*, 2012, **335**, 442-444.
332. H. Liu, H. Wang and X. Zhang, *Advanced Materials*, 2015, **27**, 249-254.

333. K. Celebi, J. Buchheim, R. M. Wyss, A. Droudian, P. Gasser, I. Shorubalko, J.-I. Kye, C. Lee and H. G. Park, *Science*, 2014, **344**, 289-292.
334. M. Hu and B. Mi, *Environmental Science & Technology*, 2013, **47**, 3715-3723.
335. S. Mozia, *Separation and Purification Technology*, 2010, **73**, 71-91.
336. H. Wang, Z. Dong and C. Na, *ACS Sustainable Chemistry & Engineering*, 2013, **1**, 746-752.
337. S. R. Lewis, S. Datta, M. Gui, E. L. Coker, F. E. Huggins, S. Daunert, L. Bachas and D. Bhattacharyya, *Proceedings of the National Academy of Sciences*, 2011, **108**, 8577-8582.
338. S. P. Albu, A. Ghicov, J. M. Macak, R. Hahn and P. Schmuki, *Nano Letters*, 2007, **7**, 1286-1289.
339. B. Sensale-Rodriguez, R. Yan, S. Rafique, M. Zhu, W. Li, X. Liang, D. Gundlach, V. Protasenko, M. M. Kelly, D. Jena, L. Liu and H. G. Xing, *Nano Letters*, 2012, **12**, 4518-4522.
340. J. Liu, M. Beals, A. Pomerene, S. Bernardis, R. Sun, J. Cheng, L. C. Kimerling and J. Michel, *Nat Photon*, 2008, **2**, 433-437.
341. A. Julbe, D. Farrusseng and C. Guizard, *Journal of Membrane Science*, 2001, **181**, 3-20.
342. B. Guo, E. V. Pasco, I. Xagorarakis and V. V. Tarabara, *Separation and Purification Technology*, 2015, **149**, 245-254.
343. H. A. Shawky, S.-R. Chae, S. Lin and M. R. Wiesner, *Desalination*, 2011, **272**, 46-50.
344. A. V. Dudchenko, J. Rolf, K. Russell, W. Duan and D. Jassby, *Journal of Membrane Science*, 2014, **468**, 1-10.
345. C. D. Vecitis, M. H. Schnoor, M. S. Rahaman, J. D. Schiffman and M. Elimelech, *Environmental Science & Technology*, 2011, **45**, 3672-3679.
346. W. Duan, A. Dudchenko, E. Mende, C. Flyer, X. Zhu and D. Jassby, *Environmental Science: Processes & Impacts*, 2014, **16**, 1300-1308.
347. M. S. Rahaman, C. D. Vecitis and M. Elimelech, *Environmental Science & Technology*, 2012, **46**, 1556-1564.
348. G. Gao and C. D. Vecitis, *ACS Applied Materials & Interfaces*, 2012, **4**, 1478-1489.
349. C. F. de Lannoy, D. Jassby, D. D. Davis and M. R. Wiesner, *Journal of Membrane Science*, 2012, **415-416**, 718-724.
350. Z. Chu, Y. Feng and S. Seeger, *Angewandte Chemie International Edition*, 2015, **54**, 2328-2338.
351. Y. Zhu, D. Wang, L. Jiang and J. Jin, *NPG Asia Mater*, 2014, **6**, e101.
352. B. Wang, W. Liang, Z. Guo and W. Liu, *Chemical Society Reviews*, 2015, **44**, 336-361.
353. X. Deng, L. Mammen, H.-J. Butt and D. Vollmer, *Science*, 2012, **335**, 67-70.
354. Z. Shi, W. Zhang, F. Zhang, X. Liu, D. Wang, J. Jin and L. Jiang, *Advanced Materials*, 2013, **25**, 2422-2427.
355. B. Su, W. Guo and L. Jiang, *Small*, 2015, **11**, 1072-1096.
356. S. Wang and L. Jiang, *Advanced Materials*, 2007, **19**, 3423-3424.
357. A. Lafuma and D. Quere, *Nat Mater*, 2003, **2**, 457-460.
358. T. Sun, L. Feng, X. Gao and L. Jiang, *Accounts of Chemical Research*, 2005, **38**, 644-652.
359. X.-M. Li, D. Reinhoudt and M. Crego-Calama, *Chemical Society Reviews*, 2007, **36**, 1350-1368.
360. X. Zhang, F. Shi, J. Niu, Y. Jiang and Z. Wang, *Journal of Materials Chemistry*, 2008, **18**, 621-633.
361. Q. Li, P. Xu, W. Gao, S. Ma, G. Zhang, R. Cao, J. Cho, H.-L. Wang and G. Wu, *Advanced Materials*, 2014, **26**, 1378-1386.
362. L. Feng, S. Li, Y. Li, H. Li, L. Zhang, J. Zhai, Y. Song, B. Liu, L. Jiang and D. Zhu, *Advanced Materials*, 2002, **14**, 1857-1860.

363. L. Feng, Z. Zhang, Z. Mai, Y. Ma, B. Liu, L. Jiang and D. Zhu, *Angewandte Chemie*, 2004, **116**, 2046-2048.
364. M. Liu, S. Wang, Z. Wei, Y. Song and L. Jiang, *Advanced Materials*, 2009, **21**, 665-669.
365. Z. Xue, S. Wang, L. Lin, L. Chen, M. Liu, L. Feng and L. Jiang, *Advanced Materials*, 2011, **23**, 4270-4273.
366. Q. Wen, J. Di, L. Jiang, J. Yu and R. Xu, *Chemical Science*, 2013, **4**, 591-595.
367. F. Zhang, W. B. Zhang, Z. Shi, D. Wang, J. Jin and L. Jiang, *Advanced Materials*, 2013, **25**, 4192-4198.
368. W. Zhang, Y. Zhu, X. Liu, D. Wang, J. Li, L. Jiang and J. Jin, *Angewandte Chemie International Edition*, 2014, **53**, 856-860.
369. J. A. Howarter and J. P. Youngblood, *Advanced Materials*, 2007, **19**, 3838-3843.
370. J. A. Howarter and J. P. Youngblood, *Macromolecular Rapid Communications*, 2008, **29**, 455-466.
371. L. Zhang, Y. Zhong, D. Cha and P. Wang, *Sci. Rep.*, 2013, **3**.
372. L. Zhang, Z. Zhang and P. Wang, *NPG Asia Mater*, 2012, **4**, e8.
373. B. Wang and Z. Guo, *Chemical Communications*, 2013, **49**, 9416-9418.
374. D. Tian, X. Zhang, Y. Tian, Y. Wu, X. Wang, J. Zhai and L. Jiang, *Journal of Materials Chemistry*, 2012, **22**, 19652-19657.
375. B. Xue, L. Gao, Y. Hou, Z. Liu and L. Jiang, *Advanced Materials*, 2013, **25**, 273-277.
376. Z. Xu, Y. Zhao, H. Wang, X. Wang and T. Lin, *Angewandte Chemie*, 2015, **127**, 4610-4613.
377. L. Zhang, J. Wu, M. N. Hedhili, X. Yang and P. Wang, *Journal of Materials Chemistry A*, 2015, **3**, 2844-2852.
378. N. S. Lewis, *Science*, 2007, **315**, 798-801.
379. T. Oki and S. Kanae, *Science*, 2006, **313**, 1068-1072.
380. Z. Fang, Y.-R. Zhen, O. Neumann, A. Polman, F. J. García de Abajo, P. Nordlander and N. J. Halas, *Nano Letters*, 2013, **13**, 1736-1742.
381. Z. Wang, Y. Liu, P. Tao, Q. Shen, N. Yi, F. Zhang, Q. Liu, C. Song, D. Zhang, W. Shang and T. Deng, *Small*, 2014, **10**, 3234-3239.
382. R. W. Wood, *Philosophical Magazine Series 6*, 1902, **4**, 396-402.
383. O. Neumann, A. S. Urban, J. Day, S. Lal, P. Nordlander and N. J. Halas, *ACS Nano*, 2013, **7**, 42-49.
384. L. Zhang, B. Tang, J. Wu, R. Li and P. Wang, *Advanced Materials*, 2015, DOI: 10.1002/adma.201502362, n/a-n/a.
385. S. J. Kim, S. H. Ko, K. H. Kang and J. Han, *Nat Nano*, 2010, **5**, 297-301.
386. S. J. Kim, S. H. Ko, K. H. Kang and J. Han, *Nat Nano*, 2013, **8**, 609-609.